Chemical characterizations and molecular dynamics simulations on different rejuvenators for aged bitumen recycling

Ren, S.; Liu, X.; Lin, P.; Erkens, S.; Gao, Y.

DOI
10.1016/j.fuel.2022.124550

Publication date
2022

Document Version
Final published version

Published in
Fuel

Citation (APA)
Ren, S., Liu, X., Lin, P., Erkens, S., & Gao, Y. (2022). Chemical characterizations and molecular dynamics simulations on different rejuvenators for aged bitumen recycling. *Fuel*, *2022*(324), 1-17. Article 124550. https://doi.org/10.1016/j.fuel.2022.124550

Fuel 324 (2022) 124550

Contents lists available at ScienceDirect

Fuel

journal homepage: www.elsevier.com/locate/fuel

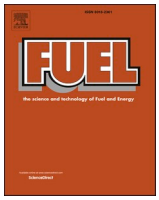

Full Length Article

Chemical characterizations and molecular dynamics simulations on different rejuvenators for aged bitumen recycling

Shisong Ren [a,b,*], Xueyan Liu [a], Peng Lin [a], Sandra Erkens [a], Yangming Gao [a]

[a] Section of Pavement Engineering, Faculty of Civil Engineering & Geosciences, Delft University of Technology, Stevinweg 1, 2628 CN Delft, the Netherlands
[b] State Key Laboratory of Heavy Oil Processing, China University of Petroleum, Qingdao 266580, PR China

ARTICLE INFO

Keywords:
Molecular models
Rejuvenators
Chemical characterizations
Molecular dynamics simulation
Thermodynamics properties

ABSTRACT

Molecular dynamics (MD) simulation is an advanced tool to explore the interaction mechanism between aged bitumen and rejuvenators at the nanoscale. However, the general MD molecular structures of rejuvenators led to the lower quantify and inaccuracy of the simulation outputs. This study aims at developing more realistic molecular models to represent the generic rejuvenators for MD simulation of aged bitumen recycling. Four types of rejuvenators (bio-oil, engine-oil, naphthenic-oil, and aromatic-oil) are characterized in terms of element analysis, functional groups distribution observed from Attenuated total reflectance-Fourier-transform infrared (ATR-FTIR) spectroscopy, and average molecular weight. Afterward, the average molecular structures of rejuvenators are determined and validated. Further, the MD simulations are performed to predict the energetic, dynamic, volumetric, and structural properties of various rejuvenators. Based on the chemical characteristics, the average chemical formula of bio-oil, engine-oil, naphthenic-oil, and aromatic-oil is derived as $C_{19}H_{36}O_2$, $C_{22}H_{44}$, $C_{26}H_{48}$, $C_{30}H_{40}$. From MD simulations, the ranking of density and glass transition temperature for four different rejuvenators is AO > NO > BO > EO, which is same as the experimental results. It proves that the established average molecular structures of four rejuvenators are reasonable. Various rejuvenators display different thermodynamics and structural properties. The aromatic-oil exhibits the highest potential energy, cohesive energy density, and solubility parameter. Besides, the order of expansion coefficient and diffusion coefficient of the four rejuvenators is the same as BO > EO > NO > AO, while the viscosity presents the opposite sequence. Moreover, the fractional free volume values follow EO > BO > NO > AO. The occurrence probability between bio-oil and aromatic-oil molecules is higher than engine-oil and naphthenic-oil. This study develops the representative average molecular models for generic rejuvenators and helps understand the difference in chemo-physical and thermodynamics properties among various rejuvenators.

1. Introduction

With the gradual depletion of fossil energy, the reuse of aged bitumen in reclaimed asphalt pavement (RAP) is gaining more attention during the maintenance and reconstruction of flexible asphalt roads [1–3]. Economic and environmental sustainability are achieved when the damaged asphalt road can be repaired without consuming any new bituminous material [4]. However, there are lots of challenges to recover the deteriorated performance of bitumen due to the severe aging during its service life. The utilization of highly stiff-and-brittle aged bitumen with no rejuvenation process would accelerate the cracking and moisture damage, leading to a shortening service life of recycled asphalt pavement [5].

Regarding the chemical aging mechanism of bitumen, the variations of bitumen components and functional groups distribution are mainly observed. On the one hand, the bitumen components are generally divided into four groups (saturates (S), aromatics (A), resins (R), and asphaltenes (As) fractions) on basis of polarity, solubility, and molecular weight [6]. The oxidative aging results in the components' conversion in bitumen through both physical evaporation and chemical oxidative reaction ways [7]. The light oily fractions (saturates and aromatics) continue to transfer to heavy molecules (resins and asphaltenes), and the SARA fractions distribution changes directly cause the performance upgrading (rutting resistance) and deterioration (cracking potential and moisture sensitivity) [8,9]. On the other hand, the dosage signal of oxygen-containing functional groups (carbonyl, sulfoxide, etc.)

* Corresponding author.
E-mail address: Shisong@tudelft.nl (S. Ren).

https://doi.org/10.1016/j.fuel.2022.124550
Received 5 March 2022; Received in revised form 19 April 2022; Accepted 7 May 2022

associated with oxidation reactions enlarges significantly as the aging degree deepens [10]. It promotes the increment of molecular polarity, intermolecular interaction as well as agglomeration potential between bitumen molecules [11].

Nowadays, numerous rejuvenators are developed and selected to reactivate the mechanical performance of aged bitumen by the principle of supplementing the saturates and aromatics fractions as well as diluting the generated polar products during aging. Different kinds of recycling agents from bioresources (such as vegetable oils [12], waste cooking oils [1], and other bio-oils [13]) and petroleum-based products (like engine oils [5], naphthenic oils [14], aromatic oils [15], etc.) have been proved to be efficient in improving the low-temperature cracking resistance, fatigue life, workability, and durability of aged bitumen and mixture [16,17]. The rejuvenation efficiency of rejuvenators on the rheological and mechanical performance of aged bitumen strongly depends on the rejuvenator type and components [14,18]. To this end, the American National Center for Asphalt Technology (NCAT) categorized the rejuvenators into five groups based on their chemical characteristics and material resources, including the paraffinic-oils, naphthenic-oils, aromatic extracts, triglycerides/fatty acids, and tall oils [14]. Hamzeh et al. detected the distinct difference in chemical properties between five recycling agents and found that the rejuvenation efficiency on mechanical properties and moisture susceptibility significantly depends on the recycling agents [8,18].

Although it is easier to distinguish the difference in rejuvenation efficiency between various rejuvenators on SARA components, functional groups distribution, performance grade as well as microstructure morphology of aged bitumen, the underlying mechanism regarding the interaction between aged bitumen and different rejuvenators are still not clear, which is difficult to monitor at the macroscale point [19]. Molecular dynamics simulation is proved to be a powerful tool to help researchers fundamentally understand the molecular interaction and predict the essential thermodynamics properties of materials at the nanoscale [20]. The proposal of representative 12-components model of bitumen markedly promotes the application of the MD simulation method in bituminous materials, including performance prediction of a virgin [21], modified [22] and aged bitumen [23], diffusion [24], and self-healing behaviors [25], as well as the interfacial adhesion of aggregate-bitumen system [26,27]. Meanwhile, previous studies applied the MD simulation on exploring the rejuvenator influence on thermodynamics properties and microstructure of aged bitumen [28,29]. During MD simulations, the molecular structures of rejuvenators as important input elements directly affect the accuracy of simulation outputs. Fig. 1 listed the typical molecular structures of rejuvenators normally used in MD simulations. A single molecular formula $C_{12}H_{16}$ containing polar benzene ring, saturate naphthenic and alkyl hydrocarbons is the common model used as the molecular structure of rejuvenator [30,31]. Meanwhile, the molecular structure of $C_{10}H_{18}O_2$ was utilized to represent the sunflower oil [32]. The aromatic-based model with indole group (C_8H_9N) and alkyl-based model containing amide ($C_{16}H_{32}NO$) were also built, in which the polar aromatic cyclic and long-chain alkyl hydrocarbons are the main body of rejuvenator molecules connected with the polar functional group of indole or amide [24,33]. In addition, Sun and Wang [34] divided the molecular structures of rejuvenators into four categories, cyclic saturate, straight saturate, naphthene aromatic, and polar aromatic.

Due to the complicated and variable components in different rejuvenators, the existed molecular structures of rejuvenators are mostly determined by experience based on literature reports rather than detailed chemical characterizations. This "unrigorous" estimation method must lead to the huge difference between MD simulation outputs and experimental results. Moreover, the authentic rejuvenation mechanism at the atomic level is still unclear, and it would hinder the classification, optimization selection, and proper design of efficient rejuvenators for aged bitumen recycling. Further, few studies focus on the comparison of pure rejuvenators using multi-scale methods, which hardly prescribes the right medicine (rejuvenator) to different kinds of aged binders. Therefore, it is of significance to systematically conduct the chemical characterizations on generic rejuvenators to determine the representative molecular structures of different rejuvenators for MD simulation. Furthermore, it is also necessary to fundamentally investigate and compare the chemical, physical and thermodynamic properties of the generic rejuvenators.

2. Research objectives and methodologies

The main objective of this study is to develop representative molecular models for commonly-used generic rejuvenators and predict their thermodynamics behaviors at the atomic level with MD simulations.

Fig. 2 shows the research framework of this paper. Firstly, the elemental composition, functional groups distribution, and average molecular weight of four basic commonly-used rejuvenators (bio-oil, engine oil, naphthenic-oil, and aromatic-oil) were measured to provide the basis to determine their average molecular structures. Afterward, the MD simulation was adopted on the average molecular models to fundamentally predict and compare the nanoscale properties of various rejuvenators, while experimental tests were conducted to validate the reliability of average molecular models of rejuvenators, including the density and glass transition temperature. Finally, other crucial thermodynamics parameters (Energetic parameters, cohesive energy density, solubility parameter, diffusion behavior, volumetric and structural characteristics) of various rejuvenators were predicted and compared at the nanoscale.

3. Materials and experimental methods

3.1. Raw materials

In this study, four types of generic rejuvenators were selected, including the bio-oil (BO), engine-oil (EO), naphthenic-oil (NO), and aromatic-oil (AO), which are all purchased from the market. The bio-oil with the color of pale yellow is the rap-oil, while the engine oil (brown liquid), naphthenic oil (transparent liquid), and aromatic oil (dark-brown semisolid) are all petroleum-based products. Table 1 lists the physical indices of four rejuvenators. The density order from high to low

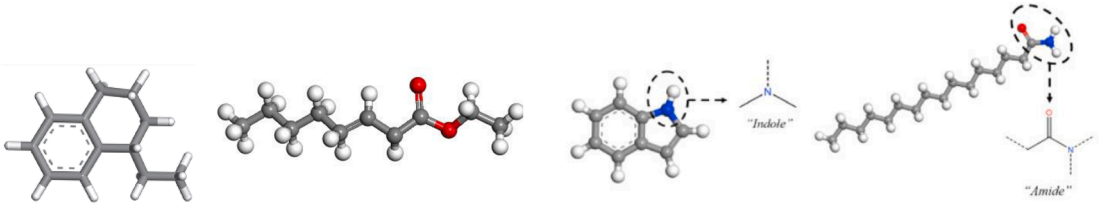

(a) $C_{12}H_{16}$ (b) $C_{10}H_{18}O_2$ (c) C_8H_9N (d) $C_{16}H_{32}NO$

Fig.1. Typical molecular structures of rejuvenators used in MD simulations [30–34].

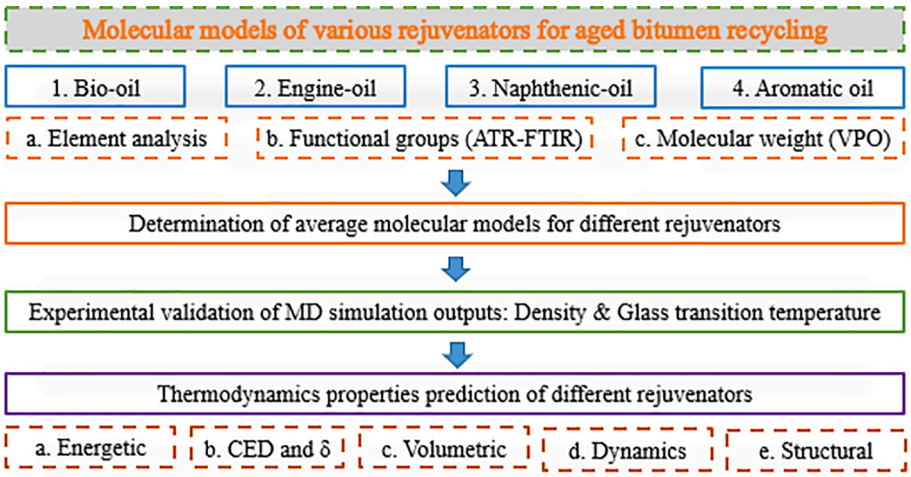

Fig.2. Research schemes and methodologies.

Table 1
The basic properties of various rejuvenators.

Items	BO	EO	NO	AO
Color	Pale yellow	brown	transparent	Dark-brown
Density (25℃, g/cm^3)	0.911	0.833	0.875	0.994
Density (60℃, g/cm^3)	0.899	0.814	0.852	0.978
Viscosity (25℃, cP)	50	60	130	63,100
Flash point (℃)	265–305	>225	>230	>210

for the four rejuvenators is as AO > BO > NO > EO, while the magnitude of dynamic viscosity at 25℃ is AO > NO > EO > BO. It should be mentioned that the AO rejuvenator exhibits a similar density as virgin bitumen (about 1.0 g/cm^3) [35], and it has a higher viscosity than the other three rejuvenators.

3.2. Experimental methods

3.2.1. Element analysis

The elemental compositions of four rejuvenators, referring to the dosage of carbon (C), hydrogen (H), Sulfur (S), Nitrogen (N), and Oxygen (O) elements, were measured by using an elemental analyzer (Vario EL III) manufactured from the Elementar Corp., Germany. The machine was firstly calibrated by testing the element distribution of one reference substance (sulfanilamide). Afterward, about 10-mg rejuvenator was wrapped in a thin capsule and put into a sample tank for further sufficient oxidization and combustion. The gas products were separated and detected to determine the content of different elements [14]. The oxygen concentration (O%) was calculated by (100-C%-H%-S%-N%) with an assumption that there was no other element type existing in these rejuvenators.

3.2.2. Attenuated total reflectance-Fourier-transform infrared (ATR-FTIR) spectroscopy

The molecular structures of organic rejuvenators are composed of hydrocarbon chains and polar functional groups with heteroatoms [10]. In this study, the functional groups in the molecular structure of four rejuvenators were monitored by using the ATR-FTIR device (Waltham, MA, USA) with the wavenumber region of 600–4000 cm^{-1} at room temperature. The scan number for each sample was 12 and at least three parallel tests were measured to ensure data accuracy.

3.2.3. Vapor pressure Osmometry (VPO) test

In this study, the average molecular weight of rejuvenators was obtained with the Vapor Pressure Osmometry (VPO) test, which was the conventional way to measure the molecular weight of petroleum distillates [36]. The engine-oil, naphthenic-oil, and aromatic-oil rejuvenators were all petroleum-based products with a molecular weight lower than 1000 g/mol, which could be detected by using Gel Permeation Chromatography (GPC). Fig. 3 illustrates the working principle, test device, and rejuvenator specimens in the VPO test, which measures the average molecular weight according to the difference in vapor pressure due to the addition of solute to a pure solvent. The VPO device adopted here was a Knauer osmometer (Knauer, Berlin-Heidelberg, West Germany), shown in Fig. 3**b**. Toluene was used as a solvent, while benzile was the calibration substance. Before testing, different benzile/toluene solutions with various concentrations of 0.005, 0.01, 0.015, and 0.02 mol/kg were prepared, and the standard solution curve between the VPO response parameter v/c and relative mass molarity c of solute could be drawn. Meanwhile, rejuvenator/toluene solutions with specific mass ratios were manufactured (see Fig. 3**c**), and the corresponding VPO response v/c values of rejuvenator solutions were measured. Lastly, the relative mass molarity of the rejuvenator in solution was determined in a standard curve, and the average molecular weight of solvent (rejuvenator) could be calculated.

3.2.4. Pycnometer density measurement

The density is the most popular index for validating the reasonability of molecular structures and MD simulation settings (Forcefield type, time step, energy summation method, etc.). In this study, the density values of rejuvenators were tested with the capillary-stoppered pycnometer method at 25 and 60℃ according to the standard of EN 15,326 [35].

3.2.5. Differential scanning calorimetry (DSC) test

In this study, the glass transition temperatures of different rejuvenators were determined based on the heat capacity variation measured by the DSC device from PerkinElmer company. About 10-mg rejuvenator specimen was encased in an aluminum plate and put in a sample room. The testing program was to heat the rejuvenator sample to 160 ℃ to fully relax the rejuvenator molecules firstly, which was then cooled down to the minimum temperature of −70 ℃ with a constant cooling rate of 10 ℃/min. The heat flow change as a function of temperature was recorded to obtain the glass transition temperatures of four generic rejuvenators.

3.2.6. Dynamic viscosity test

The dynamic viscosity values of pure rejuvenators were measured with a rotational viscometer (RV) at different temperatures of 25, 40, 60, and 100℃ according to the standard of AASHTO T316-13. The rotor spinning rate was 20 rad/s and the viscosity was obtained when the holding time was longer than 30 min.

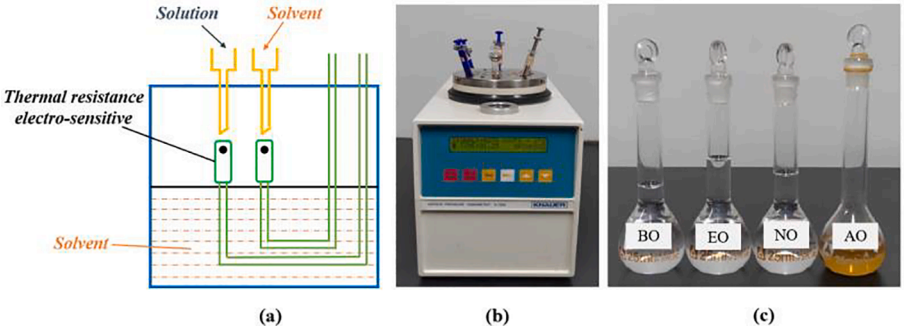

Fig.3. The working principle, test device, and rejuvenator samples in the VPO test.

4. Experimental results and discussion

4.1. Elemental compositions of rejuvenators

Element components are of significance to determine the atom numbers and whole molecular formula together with known molecular weight. Table 2 lists the elemental compositions (N, C, H, S, and O) of four rejuvenators. As expected, the rejuvenators are mainly composed of carbon and hydrogen elements (hydrocarbons). Besides, it is depicted that in all rejuvenators, the N and S element contents are markedly lower than C and H. Besides, the oxygen dosage in engine-oil, naphthenic-oil and aromatic-oil are less than 0.5%, while high oxygen content of 11.36% is detected in bio-oil rejuvenator. Herein, the oxygen-containing functional groups exist in the molecular structure of bio-oil rejuvenator, and the chemical components in three petroleum-based rejuvenators are hydrocarbons without heteroatom functional groups.

The ratio of hydrogen to carbon element (H/C) is utilized to estimate the unsaturation degree of hydrocarbons. The higher the H/C ratio is, the larger the saturation degree is. Similarly, the ratio of oxygen to carbon element (O/C) is calculated to assess the concentration of oxygen-containing functional groups in rejuvenators. Table 2 displays the H/C and O/C values of four rejuvenators. The engine-oil has the highest H/C ratio, indicating that the molecular structure of engine-oil presents the largest saturation degree. Besides, the bio-oil and naphthenic-oil show a similar H/C value, while the H/C value of aromatic-oil is the lowest. It means that the aromatic oil exhibits the strongest degree of unsaturation, and there are plenty of unsaturated hydrocarbons in aromatic oil, such as the olefin, alkyne, and aromatic rings.

4.2. Functional groups distribution

Fig. 4 illustrates the functional groups' distribution of different rejuvenators. It can be seen that these four rejuvenators have the same strong absorbance peaks at 2920 and 2853 cm^{-1}, which represents the C–H stretch of methylene (–CH_2-) and methyl (–CH_3) in alkanes, respectively. Meanwhile, the characteristic peaks at 1456 and 1376 cm^{-1} are observed in FTIR curves of all rejuvenators, which refer to the C–H bend of –CH_2- and –CH_3 groups. Besides, the absorbance peak at 745 cm^{-1} is resulted from the C–H bend of –CH_2- in alkanes with more than four methylene terms.

It is depicted that the engine-oil and naphthenic-oil have no additional characteristic peak, indicating that their main chemical components are saturated hydrocarbons without heteroatom functional groups. However, the functional groups' distribution in bio-oil is significantly different from other petroleum-based rejuvenators. The strong characteristic peaks at 1750 and 1160 cm^{-1} are probed, which come from the C = O and C-O-C stretch in esters, respectively. Hence, the ester group exists in the molecular structure of bio-oil, and the same phenomenon was observed in previous studies [28,29]. In addition, the weak peaks at 1235 and 1096 cm^{-1} are due to the C–C(O)-C stretch of acetates and C–C stretch of ketone in esters. Interestingly, a small peak at 3007 cm^{-1} is observed, which is related to the -O–H stretch of hydroxyl in the molecular structure of fatty acid in bio-oil. It is worth noting that the peak area of –OH is smaller than ester groups, showing that the chemical component in bio-oil is mostly ester with long-chain alkanes. Regarding the aromatic-oil, the specific absorbance peaks occur at 1600, 868, and 811 cm^{-1}. The characteristic peak at 1600 cm^{-1} represents the C = C stretch of aromatic rings, while the peaks at 868 and 811 are both from the C–H bend (meta and para) in aromatic rings. It can be summarized that the aromatic-oil is composed of hydrocarbons with aromatic rings, and there is no heteroatom functional group observed in aromatic-oil rejuvenator.

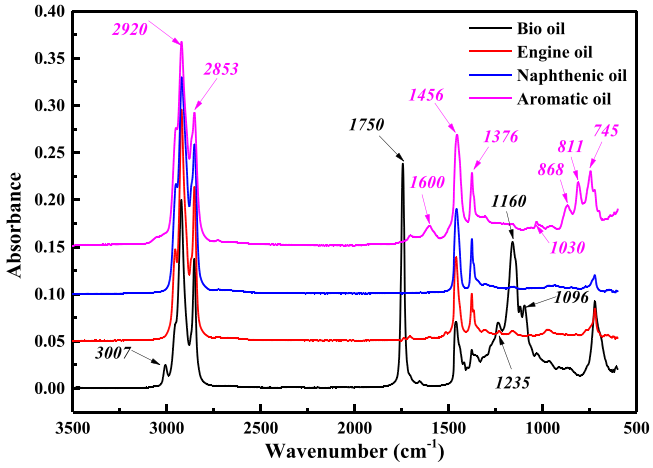

Fig.4. The FTIR results of different rejuvenators.

4.3. Average molecular weight

Fig.5 displays the VPO curve of a linear relationship between the v/c parameter and solute concentration, and the correlation function is obtained. The v/c values of rejuvenator solutions with specific mass fractions (rejuvenator/solvent) were measured and the corresponding results are listed in Table 3. Based on the standard solution curve and v/c value, the related points of four rejuvenator solutions are found and marked in Fig. 5 Afterward, the relative mass molarity of rejuvenator in

Table 2
Elemental compositions in various rejuvenators.

Rejuvenators	N%	C%	H%	S%	O%	H/C	O/C
Bio-oil	0.15	76.47	11.96	0.06	11.36	1.88	0.1114
Engine-oil	0.23	85.16	14.36	0.13	0.12	2.02	0.0011
Naphthenic-oil	0.12	86.24	13.62	0.1	0.1	1.90	0.0009
Aromatic-oil	0.55	88.01	10.56	0.48	0.4	1.44	0.0034

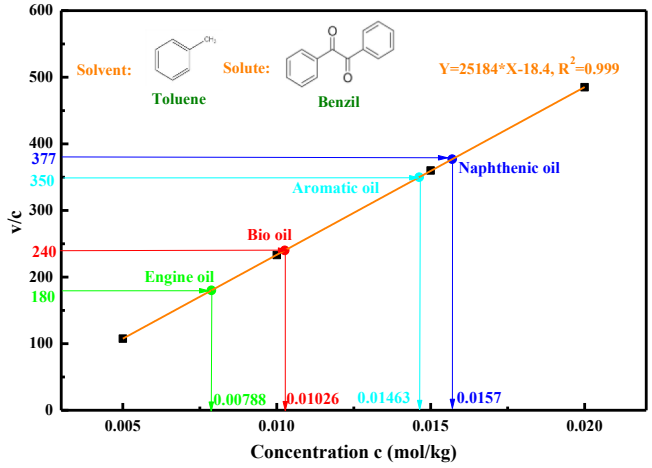

Fig.5. The VPO results of different rejuvenators.

Table 3
The VPO parameters and average molecular weight of various rejuvenators.

Rejuvenators	Bio-oil	Engine-oil	Naphthenic-oil	Aromatic-oil
m_r (g)	0.0654	0.0577	0.1234	0.0710
m_s (g)	21.8250	23.0800	22.4384	11.8334
v/c	240	180	377	350
c (mol/kg)	0.01026	0.00788	0.0157	0.01463
Mn (g/mol)	286.43	316.48	357.06	409.99

each solution is determined as 0.01026 (bio-oil), 0.00788 (engine-oil), 0.0157 (naphthenic-oil) and 0.01463 (aromatic-oil) mol·kg^{-1}. The average molecular weight of pure rejuvenators can be calculated according to **Eq.1.**

$$M_n = \frac{m_r}{c^* m_s} \quad (1)$$

where M_n is the average molecular weight of rejuvenator, g/mol; m_r and m_s represent the mass of rejuvenator and whole solution, g; while c refers to the mass molarity of pure rejuvenator in a solvent, mol/g.

The average molecular weight values of pure rejuvenators are summarized in Table 3. For each rejuvenator solution, the v/c value was measured at least 5 times, and the Mn of the rejuvenator shown in Table 3 is an average value for several parallel tests. It indicates that the Mn values of all rejuvenators are lower than 500 g/mol, which is close to the reported average molecular weight of saturate and aromatic fractions in bitumen [37]. The increasing molecular weight is the key reason for the performance deterioration of bitumen during the aging process [10,35]. Hence, these oil products with light molecular weight are generally selected as the rejuvenators to ameliorate the molecular weight distribution and restore the macroscale performance of aged bitumen. Moreover, the ranking of average molecular weight for four rejuvenators is BO < EO < NO < AO. In detail, the Mn value of bio-oil, engine-oil, naphthenic-oil, and aromatic-oil rejuvenator is 286.43, 316.48, 357.06, and 409.99 g/mol, respectively. The average molecular weight plays an important role in determining the average molecular structure of rejuvenators.

5. Molecular dynamics simulation

5.1. Determination of molecular structures for different rejuvenators

Currently, the commonly-adopted molecular structure of rejuvenators is not accurate due to the lack of experimental evidence, which is strongly dependent on the rejuvenator resource and type [17]. In this study, the average molecular structures of four generic rejuvenators for aged bitumen recycling are determined based on several chemical properties. Firstly, the element compositions and average molecular weight are utilized to recognize the number of each atom (C, H, S, N, and O) in the molecular formula of rejuvenators. The basic principle for calculating the number of each atom is described in **Eq.2.**

$$n(X) = \frac{M_n \bullet X\%}{M(X)} \quad (2)$$

where n(X) represents the number of atom X, and X refers to the carbon (C), hydrogen (H), oxygen (O), sulfur (S), or nitrogen (N), respectively; Mn is the average molecular weight of rejuvenator, g/mol; X% shows the mass fraction of element X from element analysis, and M (X) is the relative atomic mass of atom X.

The calculated numbers of different atoms in various rejuvenators are listed in Table 4**.** The relative concentrations of elements S and N are limited in each rejuvenator, which is attributed to the desulfurization and denitrification processes of light-weight oil products (including gasoline, diesel fuel, engine-oil as well as aromatic-oil) through the physical atmosphere/vacuum distillation and chemical hydrofining methods [38]. Meanwhile, most heteroatoms (S, N, and O) are included in heavy oil or bitumen molecules. In addition, the high oxygen content of the bio-oil rejuvenator is observed because of its biological resource. Thus, the heteroatoms are not considered during the establishment of average molecular structures for all rejuvenators except for the oxygen atoms in the bio-oil rejuvenator.

From Table 4, the carbon and hydrogen elements account for the most in all rejuvenators, and that's why these rejuvenators also can be called "hydrocarbons". The number of carbon atoms in rejuvenators differs from 18.8 to 30.07, while the number of hydrogen atoms is in the region of 35.28–40.30. Meanwhile, the H/C ratio and saturation degree both differ between various rejuvenators, which results in the difference of chemo-mechanical properties between rejuvenated binders. It should be mentioned that the number of all atoms should be an integer, and the average chemical formula for bio-oil, engine-oil, naphthenic-oil, and aromatic-oil rejuvenator is $C_{19}H_{36}O_2$, $C_{22}H_{44}$, $C_{26}H_{48}$, $C_{30}H_{40}$, respectively.

However, the detailed molecular structures of rejuvenators cannot be determined because the existing form and position of these elements in different functional groups are still unknown. Previous studies employed the FTIR and Nuclear Magnetic Resonance Spectroscopy (C^{13}- or H^1-NMR) methods to distinguish the position of the carbon, hydrogen atoms as well as the heteroatoms in different functional groups [37,39]. In this study, the FTIR test was conducted to identify the functional groups in four rejuvenators. And the position of the ester functional group in the molecular structure of bio-oil was determined according to the molecular structures of bio-oil rejuvenators reported in previous studies [28,32].

Fig. 6 illustrates the molecular structures of four rejuvenators, in which the black color represents the carbon atoms, while the white and red color refers to the hydrogen and oxygen atoms, respectively. Regarding the bio-oil rejuvenator, it exhibits the ester characteristic with the straight-chain monoalkene of 19 carbon atoms. Meanwhile, the average molecular structure of an engine-oil rejuvenator consists of one cyclohexane and two saturated n-octane chains. For the naphthenic oil, the main body in its chemical structure is the saturated tricyclic alkanes, which are connected with n-hexane and n-heptane alkyl substituents.

Table 4
The calculated number of different atoms in various rejuvenators.

Rejuvenators	n(C)	n(H)	n(O)	n(S)	n(N)
Bio-oil	18.80	35.28	2.09	0.0055	0.032
Engine-oil	22.21	44.95	0.023	0.013	0.051
Naphthenic-oil	25.66	48.62	0.022	0.011	0.031
Aromatic-oil	30.07	40.30	0.103	0.062	0.161

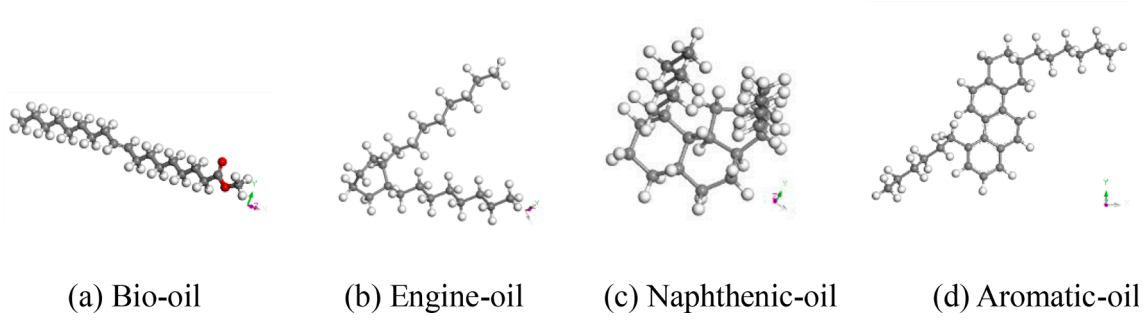

Fig. 6. The average molecular structure of various rejuvenators. (Carbon atoms: black; Hydrogen atoms: white; Oxygen atoms: red). (For interpretation of the references to color in this figure legend, the reader is referred to the web version of this article.)

Further, the aromatic-oil rejuvenator shows the distinct polycyclic aromatic hydrocarbon structure as a center, which is linked with saturated straight-chain and monocyclic alkanes. Overall, the molecular structures of rejuvenators are significantly different in terms of molecular weight, saturation degree, aromaticity, and polarity, which would be related to the differentiated rejuvenation mechanism and efficiency on aged bitumen recycling [14–17].

5.2. MD modelling and simulations

In this research, the molecular models of pure rejuvenators are built with Material Studio software through randomly incorporating 200 rejuvenator molecules into a cubic simulation box with periodic boundary conditions. The initial molecular models of four rejuvenators are shown in Fig. 7, which are then subjected to the geometry optimization procedure to minimize the system energy and avoid the overlapping of rejuvenator atoms. The COMPASSII force field is adopted throughout the whole model establishment and MD simulations of molecular models for all rejuvenators, which was proved to predict the thermodynamics properties of organic compounds efficiently [27,29,31]. In addition, the density value of all initial models was controlled as 0.1 g/cm. Afterward, the MD simulations were conducted on these initial molecular models of pure rejuvenators with the isothermal-isobaric (NPT, constant molecular number, external pressure, and temperature) ensemble to achieve the corresponding equilibrium status at 298 K and one-atmosphere pressure. The time step of 1 fs (fs) was selected, and the total simulation time was 200 picoseconds (ps). Moreover, the Nose thermostat and Andersen barostat are selected to control the temperature and pressure of pure rejuvenator systems. The summation method for van der Waals and the electrostatic term is the Ewald with the accuracy of 0.001 kcal/mol and Atom-based with the cutoff distance of 15.5 Å.

After the NPT equilibrium procedure, the canonical ensemble (NVT, constant atom number, system volume, and temperature) is performed to ensure the rejuvenator molecules are more relaxed and the whole rejuvenator model more thermodynamically stable. The NVT simulation parameters are consistent with the previous NPT process. The number of total steps is 200,000 and the Nose thermostat is chosen. The final equilibrium configurations of pure rejuvenator models are also illustrated in Fig. 7. Under the external pressure and temperature condition, the rejuvenator molecules assemble due to the molecular interaction and the whole model shrinks to a stable state. Moreover, Table 5 lists the

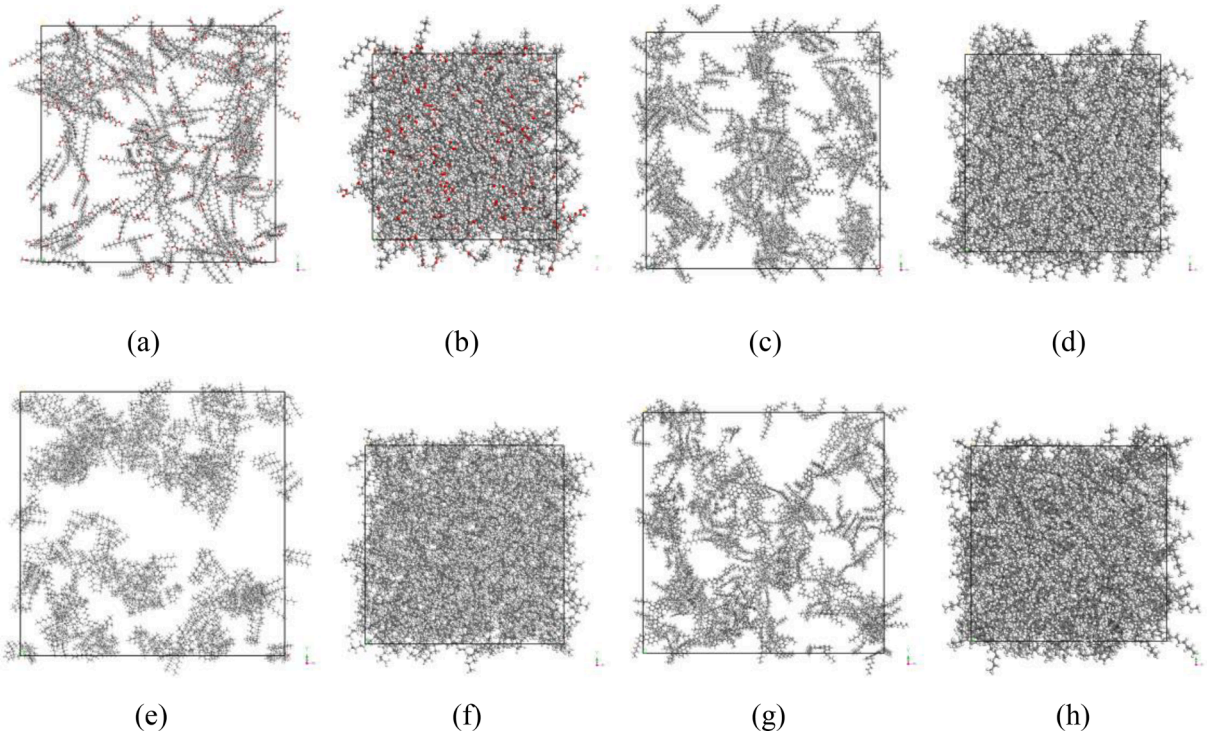

Fig.7. The initial and final molecular models of rejuvenators during MD simulations.

Table 5
The parameters in molecular models of various rejuvenators at 298 K.

Parameters	BO	EO	NO	AO
Cell volume (Å^3)	112,945	125,339	134,996	137,206
Length (Å)	48.3381	50.0451	51.2988	51.5772
Vector velocity	−0.433643	0.04906	0.21837	−0.35461
Chemical formula	$C_{19}H_{36}O_2$	$C_{22}H_{44}$	$C_{26}H_{48}$	$C_{30}H_{40}$
Net charge	−2.4331E-8	7.4506E-9	7.4506E-9	7.4506E-9
Net mass	296.495	308.594	360.67	400.64

main parameters of all equilibrium rejuvenator molecular models at 298 K. It is worth noting that the amount of rejuvenator molecules in each molecular model is the same as 200, but the cell volume (or cubic length) is significantly different with the magnitude order of BO < EO < NO < AO. The difference in cell volume between rejuvenator models is attributed to the different molecular volumes and interaction levels of rejuvenator molecules. The rejuvenator model with smaller molecular volume and stronger intermolecular attraction presents the lower cell volume [34]. Regarding the aromatic-oil rejuvenator, the polyaromatic structure increases the molecular volume significantly. Compared to the bio-oil molecule, the engine oil and naphthenic-oil molecules both have saturated cycloalkane rings, which contributes to enlarging the model volume. Meanwhile, the existence of the polar ester group in bio-oil molecules plays a crucial role in enhancing the intermolecular attractive force, which is also proved by its larger net charge.

6. Experimental validation for MD simulations

To validate the reasonability of molecular structures of four rejuvenators and the selected MD simulation parameters, the basic properties of density and glass transition temperature T_g (shown in Supplementary material) of various rejuvenators are measured in the laboratory and compared with simulation outputs.

6.1. Density validation

Fig. 8a and b illustrate the density parameter of various rejuvenators at 25 ℃ and 60 ℃ measured both from experiment and MD simulation, respectively. As expected, the increased temperature decreases the density values of rejuvenators, which is associated with enhanced molecular mobility, increased intermolecular distance, and volume expansion at high temperatures [40]. According to both experimental and simulation results, the ranking order of density for four rejuvenators is as follows: AO > NO > BO > EO. The influence factor may be the molecular structure, molecular weight, and functional groups distribution [17]. Compared with other rejuvenators, the aromatic-oil molecule has polar aromatic rings, which remarkably increases the intermolecular attractive force and tightness through the molecular agglomeration with Π-Π stacking [24,31,34]. This section is to compare the difference between MD simulation and experimental results and validate the reliability of rejuvenator molecular structures and MD simulation settings (Forcefield, time step, simulation duration, etc.). It is illustrated that the predicted density values of all pure rejuvenators strongly approach the experimental results at both 25℃ and 60℃, indicating that the established average molecular structures of four rejuvenators are reasonable and the MD simulation outputs are credible. However, there is still a little difference between the tested and predicted density of rejuvenators, especially for the bio-oil rejuvenator. Herein, the methyl oleate ($C_{19}H_{36}O_2$) molecule is selected as the average model of bio-oil, and its reported density at 20℃ was 0.874 g/cm^3 [32], which further validated that the predicted density of 0.868 g/cm^3 at 25℃ is reasonable. It should be mentioned that the bio-oil is a complicated material consisting of different fatty acids, fatty esters, and triglycerides, and the average model cannot completely represent the actual compositions. In other words, the neglected fatty acids and triglycerides influence the physical and thermodynamics properties of bio-oil [28], which may be addressed by establishing the multi-components molecular models of rejuvenators.

Regarding the engine-oil rejuvenator, the predicted density value is slightly lower than the measured one. The monocyclic saturated alkane ($C_{22}H_{44}$) molecule is adopted as the average model of engine-oil based on chemical properties of elemental fractions, functional groups distribution, and average molecular weight. However, the commercial engine-oil is composed of base oil (byproduct during the atmospheric and vacuum distillation) and functional additives (like the anti-wear agents, detergents, dispersants, and viscosity index improvers) [5,14]. Most of these additives are macromolecules with polar functional groups, which increases the density of the whole engine-oil system. Meanwhile, although the engine-oil fractions are mainly saturated alkanes and a small number of naphthene, the molecular structure of alkane (straight carbon-chain length and isomerization degree) and naphthene (type and number of saturated rings and branched chains) display an important role in affecting the chemo-physical properties of engine-oil rejuvenator.

The predicted density of the naphthenic-oil rejuvenator is slightly larger than the true value. The average molecular structure of the naphthenic-oil is a ternary-rings naphthene with two saturated alkanes branched chains ($C_{26}H_{48}$). The number of naphthene molecules with single-ring and double-rings also plays a dominant role to some extent, which is ignored in the average model. For aromatic-oil rejuvenator, the density level from MD simulation is a little smaller than the measured value. The average structure of the aromatic-oil molecule is $C_{30}H_{40}$, which includes three fused aromatic rings, one naphthenic ring, and two alkanes branched chains. Even though the co-existence of alkanes,

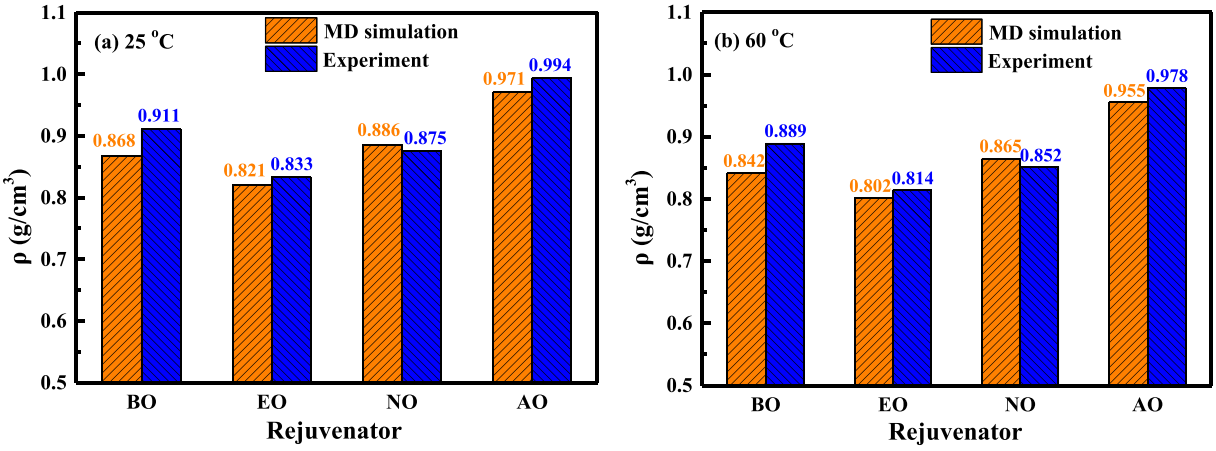

Fig.8. The result comparison of density values of various rejuvenators from MD simulation and experiment.

cycloalkanes, and aromatics molecules in aromatic-oil rejuvenator is taken into consideration in its average molecular model, the lighter and heavier fractions are all merged into one average molecule. Hence, these aromatic molecules with more than three fused aromatic-rings are overlooked here, which leads to the reduction of density value [41]. In addition, the oversight of polar heteroatoms also decreases the density of aromatic-oil [34]. All the aforementioned circumstances are widespread and inevitable when simplifying one complicated system to an average molecular model, which can be addressed through building the representative multi-components molecular model in another paper based on the chemical separation and components analysis.

7. Thermodynamics properties prediction of different rejuvenators

The molecular dynamics simulation plays a crucial role in predicting the thermodynamics properties and helping researchers understand the underlying mechanism of studied models. In this study, a series of nanoscale parameters for four rejuvenators are predicted and compared, which are hardly obtained from laboratory tests. The physical and thermodynamics properties of rejuvenators are the energetic parameters, cohesive energy density and solubility parameter, volumetric indices, molecular mobility, structural parameters, and thermophysical index.

7.1. Energetic characteristics of different rejuvenators

The energetic parameters are the first outputs from MD simulations and can be used to distinguish the energy distribution in various rejuvenators. Before that, it is necessary to be clear about the different energy terms in MD simulations with COMPASSII force field as well as their corresponding relationships, which are listed in **Eqs.3–6.**

$$E_{total} = E_{potential} + E_{kinetic} = (E_{valence} + E_{non-bond}) + E_{kinetic} = \left[\left(E_{diagonal} + E_{cross}\right) + E_{non-bond}\right] + E_{kinetic} \quad (3)$$

$$E_{diagonal} = E_{bond} + E_{angle} + E_{torsion} + E_{inversion} \quad (4)$$

$$E_{cross} = E_{stretch-stretch} + E_{stretch-bond-stretch} + E_{stretch-torsion-stretch} + E_{separated-stretch-stretch} + E_{torsion-stretch} + E_{bend-bend} + E_{torsion-bend-bend} + E_{bend-torsion-bend} \quad (5)$$

$$E_{non-bond} = E_{van\ der\ Waals} + E_{electrostatic} + E_{hydrogen\ bond} \quad (6)$$

For one simulation system with numerous molecules, two energy groups dominate during the MD simulation process, including the potential energy and kinetic energy (shown in **Eq.3**). Generally speaking, the kinetic energy is strongly connected to the simulation conditions (temperature and pressure) and molecular mobility [43]. Meanwhile, the potential energy depends on the molecular type and intermolecular interaction in the whole simulation system, which consists of the valence and non-bond terms. In detail, the valence energy comes from the molecule itself and is markedly attributed to the molecular structure. It is well-known that one molecule is composed of different atoms connecting each other through chemical bonds, which keeps active during the MD simulation. From the atomic viewpoint, one molecule can display numerous configurations, such as the stretch, bend, and torsion, all of which would result in the energy variation of molecular bond and angle. Overall, the valence energy is divided into diagonal energy (the sum of the bond, angle, torsion, and inversion energies) and cross-term energy **(Eq.5)**. Apart from the intramolecular forces, the intermolecular interaction also contributes a lot to the total energy of the whole system, which is called non-bond energy. As shown in **Eq.6**, the non-bond energy contains the van der Waals energy, electrostatic energy, and hydrogen bond energy. Besides, the non-bond energy term is distinctly related to the intermolecular displacement, amount of charge, and hydrogen bond [31,37].

Fig. 9 illustrates the main energetic parameters of four rejuvenators at the temperatures of 213 K, 298 K, and 363 K, including the potential, kinetic, non-bond, total, van der Waals, electrostatic, diagonal, and cross-terms energies. It should be mentioned that the positive values of several energetic indices are due to the regulation that the kinetic and potential energy at infinity is both equal to 0. When two molecules approach each other from the infinity point, the intermolecular attractive force does the positive work. Thus, the potential energy is lower than the infinity point (0) and shows the negative value till reaching the most stable state with the lowest potential energy. Afterward, as the molecules continue to be close, the intermolecular repulsive force dominates and the potential energy increases to overcome the repulsion. With the intermolecular distance decreasing, the potential energy enlarges even to be a positive value.

It is found that various rejuvenators display different energetic parameters, which are also influenced by simulation temperature. As the temperature increases from 213 K to 363 K, the most energetic parameters of the four rejuvenators enlarges but the cross-terms energy shows a decreasing trend. When the temperature is constant, the potential energy values of bio-oil, engine-oil, and naphthenic-oil rejuvenators are negative, while the aromatic-oil exhibits the highest positive potential energy. The reason is that the existence of condensed aromatic rings promotes the Π-Π stacking of aromatic-oil molecules, and the related intermolecular distance is decreased dramatically [31,42]. Meanwhile, the high polarity and molecular weight both intensify the intermolecular repulsive force, and the aromatic-oil molecules with a small distance would enlarge the positive energy to overcome the huge repulsion. In addition, the potential energy of bio-oil is higher than engine-oil and naphthenic-oil, which is associated with the potential hydrogen-bond in polar ester groups. The higher molecular weight and poly-cycloalkane structure of naphthenic-oil lead to larger potential energy than engine oil.

Concerning the kinetic energy, all rejuvenator molecules present positive values, and the sequence of four rejuvenators is as follows: NO > AO > EO > BO. The kinetic energy difference between rejuvenators is more significant at high temperatures, and the kinetic energy is positively correlated with the molecular mass and velocity. From Table 5, the molecular weight of naphthenic-oil and aromatic-oil are larger than engine-oil and bio-oil rejuvenators. The total energy of the rejuvenator is composed of potential energy and kinetic energy, which is illustrated in Fig. 9**d**. For bio-oil, engine-oil, and naphthenic-oil rejuvenators, the absolute values of kinetic energy are larger than potential energy, resulting in positive total energy. Regarding the aromatic-oil, both maximum potential energy and kinetic energy make its total energy is distinctly higher than other rejuvenators.

The non-bond energy is the focus of attention in MD simulations because it directly reflects the intermolecular interactions and determines the thermodynamics properties of simulation models [32,33]. The non-bond energy of various rejuvenators is shown in Fig. 9**c,** and all non-bond energy values are negative, Interestingly, the bio-oil, engine-oil, and naphthenic oil rejuvenators exhibit similar non-bond energy at all temperatures. Moreover, the non-bond energy of aromatic-oil is the highest. As mentioned before, the non-bond energy is the sum of van der Waals energy and electrostatic energy. To further explore the difference

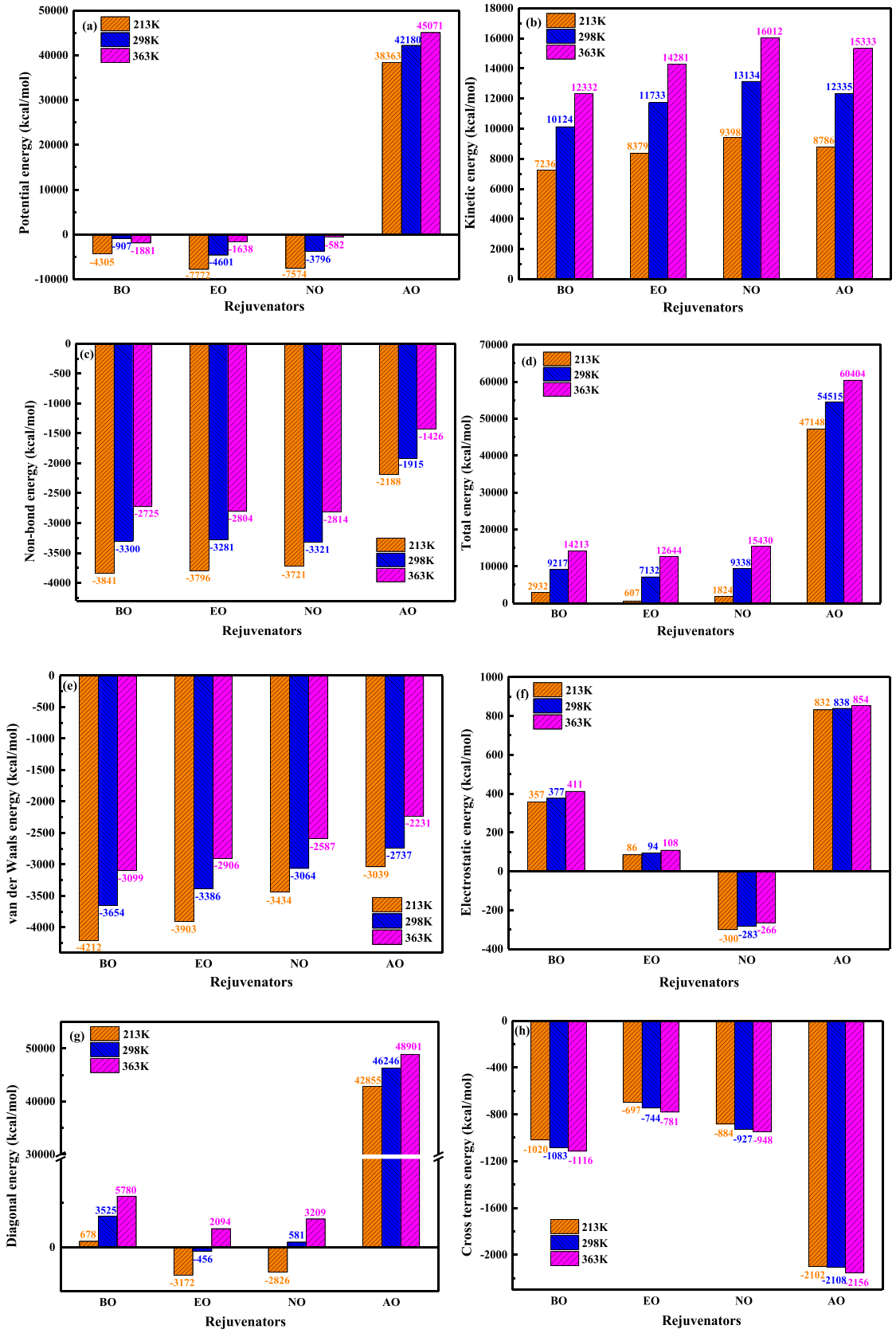

Fig.9. Different energetic parameters of various rejuvenators.

in non-bond energy between four rejuvenators, the van der Waals energy, and electrostatic energy is summarized in Fig. 9**e and f**. It is manifested that the all van der Waals energy of four rejuvenators are negative and the sequence is as BO < EO < NO < AO. Regarding the electrostatic energy, the bio-oil, engine-oil, and aromatic-oil rejuvenators display the positive values, while the naphthenic-oil shows the negative value. Meanwhile, the aromatic-oil molecules have the largest electrostatic energy, which is followed by bio-oil and engine-oil rejuvenators. The condensed aromatic rings in aromatic-oil molecules have abundant electronic charges, leading to huge electrostatic energy. For bio-oil, the high electronic charge in the polar ester group contributes to its high electrostatic energy.

Additionally, the valence energy is also included in potential energy, which contains lots of terms shown in **Eqs.4 and 5**. Here we only compare the diagonal energy and cross-terms energy of four rejuvenators, and the results are presented in Fig. 9**g and h**. Both diagonal energy and cross-terms energy of engine-oil and naphthenic oil are similar, and the latter shows slightly higher diagonal energy and lower cross-terms energy than the former, respectively. Moreover, the aromatic-oil rejuvenator exhibits the largest diagonal energy but lowest cross-terms energy, which is related to the condensed aromatic rings in aromatic-oil molecular structure. Besides, the diagonal energy and cross-terms energy of bio-oil are both in the middle between aromatic oil and naphthenic-oil. In summary, the absolute values order of diagonal energy and cross-terms energy is the same as AO > BO > NO > EO.

7.2. Cohesive energy density and solubility parameter of different rejuvenators

The cohesive energy density (CED) and solubility parameters (δ) of various rejuvenators are outputted from MD simulations following Eqs.7 and 8. The CED value is defined as the energy required to completely separate all molecules in the whole system, which is strongly associated with the intermolecular interaction (non-bond energy). Moreover, the solubility parameter difference is an important indicator for evaluating the compatibility between different matters or phases [35].

$$CED_{total} = \frac{E_{coh}}{V} \tag{7}$$

$$\delta = (CED_{total})^{0.5} = \left(\delta_{vdW}^2 + \delta_{ele}^2\right)^{0.5} \tag{8}$$

where E_{coh} and V refer to the total cohesion energy and volume of the whole rejuvenator model; δ is the total solubility parameters, which is composed of the van der Waals term δ_{vdW} and electrostatic one δ_{ele}.

Fig. 10 displays the outputted CED and δ values of four rejuvenators at 298 K. The total CED parameter is composed of the van der Waals and electrostatic terms. The van der Waals interaction plays a crucial role in determining the total CED value of each rejuvenator, which is two orders of magnitude higher than the electrostatic one. The aromatic-oil rejuvenator exhibits the largest CED value of 3.406E8 J/cm^3, followed by bio-oil (3.190E8 J/cm^3) and naphthenic-oil (2.723E8 J/cm^3). The engine-oil rejuvenator has the lowest CED (2.170E8 J/cm^3) but is close to naphthenic-oil. Meanwhile, the sequence of van der Waals CED for four rejuvenators is the same as the total one and as follows: AO > BO > NO > EO. It suggests that it is the most difficult for aromatic-oil molecules to evaporate from the main body, while the required energy for the evaporation of engine-oil and naphthenic-oil molecules is the lowest. The evaporation degree of the rejuvenator molecules may be related to the thermal aging performance of rejuvenated bitumen [7,16]. The reason for the CED difference is that the aromatic-oil molecules own the fused aromatic rings with the strongest polarity, and it strengthens the intermolecular attraction force through the Π-Π stacking way. Meanwhile, the polar ester group in the bio-oil molecule increases the intermolecular attractive interaction, which may be further enhanced through the hydrogen bonds [32]. However, the average molecular structures of engine-oil and naphthenic oil are both composed of saturated cycloalkanes and straight alkanes with less polarity. Thus, the total, van der Waals and electrostatic CED values of engine-oil and naphthenic-oil rejuvenators are lower than bio-oil and aromatic-oil rejuvenators. Interestingly, the electrostatic CED value of bio-oil is slightly higher than aromatic-oil, which may be explained through the larger charge value or smaller intermolecular distance between bio-oil molecules [28,32].

The comparison of solubility parameters between various rejuvenators shows a similar law with the CED parameter. The aromatic-oil rejuvenator has the largest δ value of 18.455, which is followed by bio-oil (17.862). Besides, the engine-oil and naphthenic-oil present the lower δ value of 16.465 and 16.501, respectively. Meanwhile, the electrostatic δ values of aromatic-oil and naphthenic-oil are approximately 3–4 times larger than engine-oil and naphthenic-oil rejuvenators. Our previous work revealed that the δ values of aged bitumen after laboratory pressure aging vessel (PAV) long-term aging processes for 20 h, 40 h, and 80 h were located in 18.5–19.5 [35], which are all larger than four rejuvenators. According to solubility theory, the smaller the solubility parameter difference (Δδ) is, the better the compatibility between different phases is. Thence, the δ value of aromatic-oil rejuvenator is the closest to the aged bitumen, followed by bio-oil and naphthenic oil rejuvenators. And the Δδ value between the engine oil and aged binders is the largest. In other words, the compatibility order of four rejuvenators with aged bitumen may be as follows: AO > BO > NO > EO,

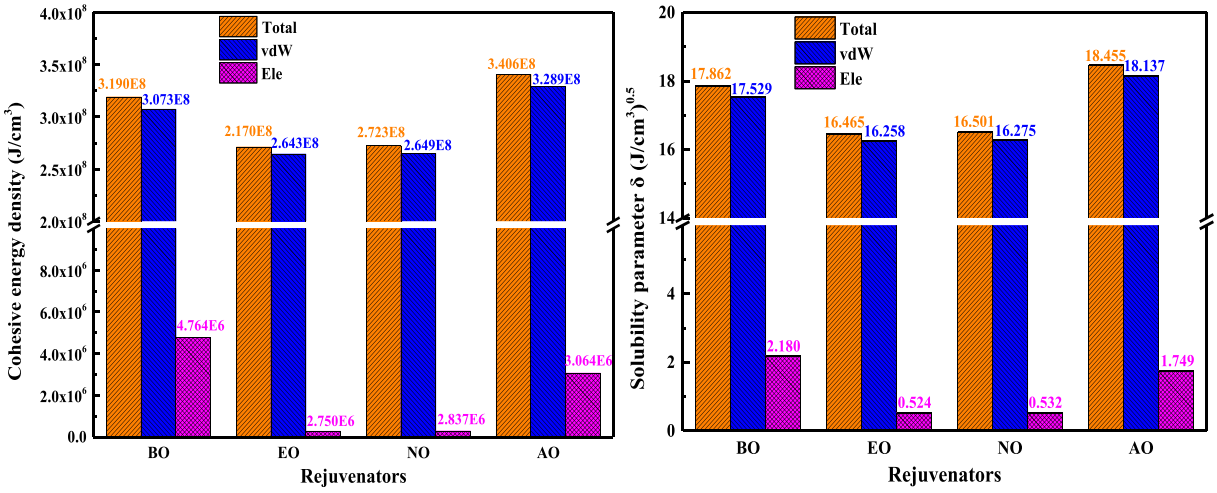

Fig.10. CED and solubility parameter of various rejuvenators at 298 K.

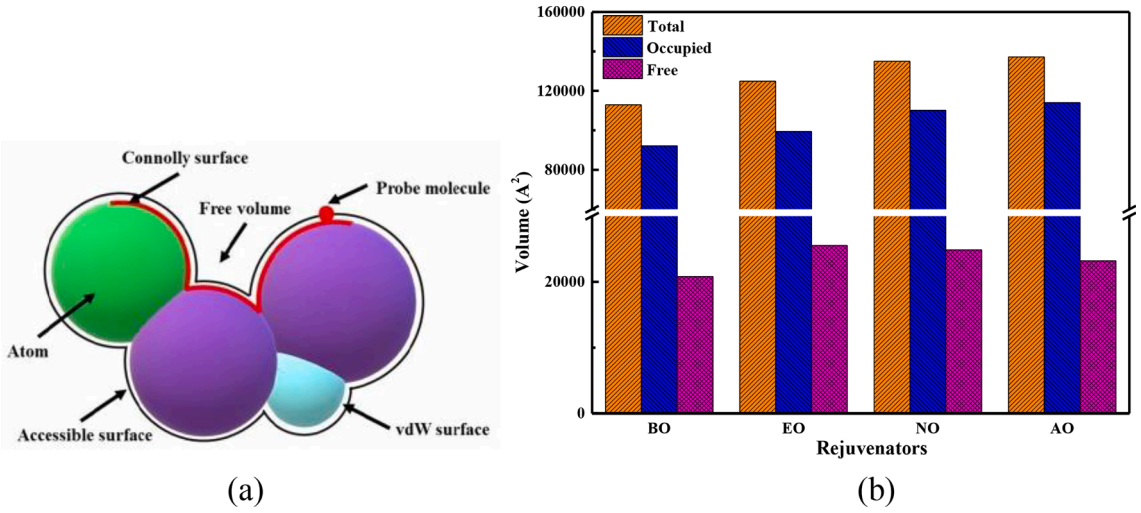

Fig.11. The volumetric parameters of different rejuvenators at 298 K.

which should be further validated in future work.

7.3. Volumetric parameters of different rejuvenators

Previous studies reported that the nanoscale microstructure was related to the macroscale relaxation and low-temperature cracking performance of bitumen [43,46]. The volumetric parameters in MD simulations contain the total, occupied, and free volume, which are illustrated in Fig. 11**a**. The total volume refers to the whole equilibrate simulation model volume, while the occupied and free volume comes from the molecular intrinsic volume and intermolecular space, respectively [43]. Fig. 11**b** shows the volumetric parameters of four rejuvenators at 298 K. Owing to the difference in molecular structures, the volumetric parameters of different rejuvenators are variable. It can be found that the bio-oil rejuvenator has the lowest total and occupied volume, followed by engine-oil and naphthenic-oil rejuvenators. Moreover, both total and occupied volumes of aromatic-oil rejuvenator are the maximum. It should be mentioned here that the molecule number in all rejuvenator models is the same as 200, thus the difference in volumetric indices is related to the molecule type and molecular interaction as well as the external factors (temperature and pressure).

As shown in Fig. 6, the main molecular structure of bio-oil, engine-oil, naphthenic-oil, and aromatic-oil rejuvenator is a straight-chain alkane with an ester group, mono-cycloalkane, polycyclic alkanes, and polycyclic aromatic hydrocarbons, respectively. The increase of cycloalkane and aromatic rings' number leads to the enlargement of molecular intrinsic volume. Meanwhile, the molecular steric hindrance is improved accordingly, which also increases the total volume of rejuvenators models. Regarding the free volume, the bio-oil rejuvenator has the lowest point, while the engine-oil rejuvenator shows the highest value, followed by the naphthenic-oil and aromatic-oil rejuvenators. The total volume (whole cubic), occupied volume (red color), and free volume (blue color) of four rejuvenators are illustrated in Fig. 12. It can be found that the occupied volume with rejuvenator molecules is the continuous phase, and the free volume is distributed as an island-like form.

Additionally, the temperature change would result in the variation of volumetric parameters of rejuvenators owing to the enlarged molecular mobility and system expansion [31,42]. To further understand and compare the temperature dependence of volumetric indices of various rejuvenators, Fig. 13 plots the influence of temperature on the total, occupied, and free volume of different rejuvenators. The van der Waals volume (V_{vdW}) is derived from the occupied volume V_o ($V_o = 1.3V_{vdW}$). The increase of temperature shows no influence on the occupied volume of the rejuvenator because of the constant mass and volume of atoms in a simulation model. On the contrary, the total and free volume of each rejuvenator both enlarge significantly with the increase of temperature. Meanwhile, the increasing trend of total and free volume is almost the same, suggesting that the effect of temperature on volumetric change of the whole rejuvenator system comes from the variation of free volume. As the temperature rises, all rejuvenator molecules obtaining more kinetic energy exhibit stronger mobility and move far away from each other, which leads to the enlargement of total and free volume [40,43]. Similar to density index, one turning point on both total and free volume curves are noticed and resulted from the phase transition around the glass transition temperature point. After the Tg value, the free volume of the rejuvenator system increases distinctly, and it may be beneficial to enhance the stress relaxation of rejuvenators.

The free volume is the most important index to determine the volume variation of the rejuvenator system [43]. However, it is difficult to

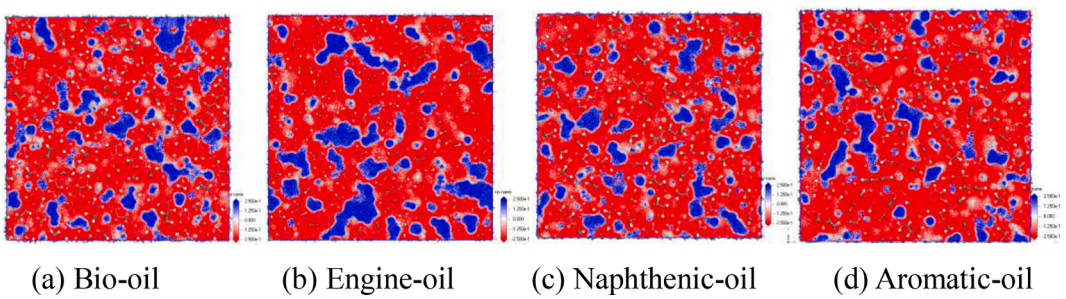

Fig.12. The schematic diagram of free volume in molecular models of rejuvenators. (Red color represents the occupied volume and the blue one is the free volume). (For interpretation of the references to color in this figure legend, the reader is referred to the web version of this article.)

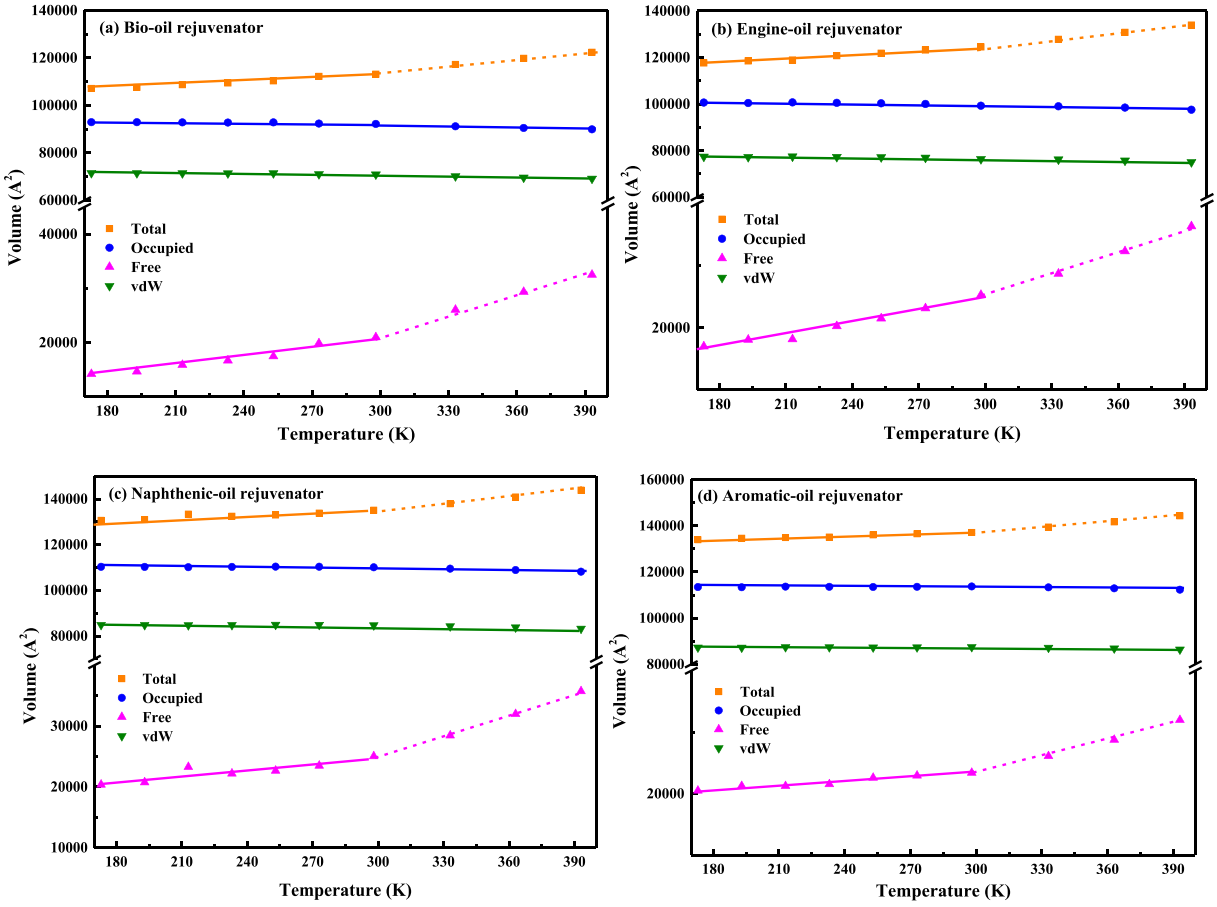

Fig.13. Influence of temperature on volumetric parameters of various rejuvenators.

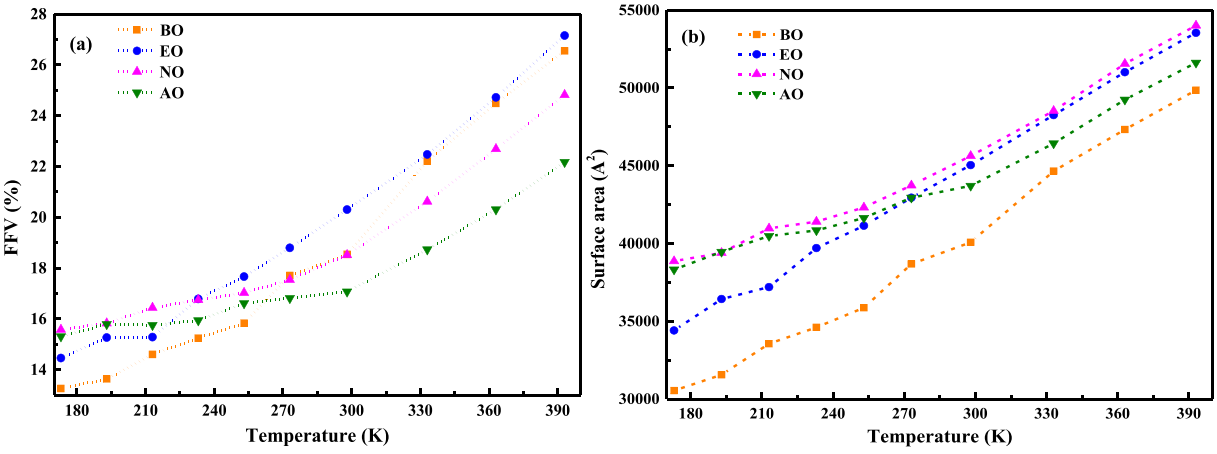

Fig.14. Influence of temperature on FFV and surface area of various rejuvenators.

directly compare the free volume of rejuvenators because their different molecular structures result in the variable occupied and total volume. Herein, an effective index, fractional free volume (FFV), is introduced to quantitatively compare the free volume terms of various rejuvenators, which is calculated as follows:

$$FFV = \frac{V - 1.3V_{vdW}}{V} = \frac{V - V_0}{V} \quad (9)$$

where FFV is the fractional free volume, %; V refers to the total volume of rejuvenator system, Å^3; V_{vdW} and V_o represent the van der Waals volume and occupied volume, Å^3, respectively.

Fig. 14 displays the FFV values of four rejuvenators as a function of temperature. The FFV values of rejuvenators enlarge as the temperature increases. Meanwhile, the increasing rate of FFV value in the high-temperatures region is more significant than that at low temperatures. When the temperature is higher than 273 K, the magnitude of FFV value for four rejuvenators is observed as follows: EO > BO > NO > AO. This sequence is opposite to the density result, in which the engine-oil rejuvenator shows the lowest density, while the aromatic-oil exhibits the highest density. From the viewpoint of rejuvenator molecular structures, the engine-oil molecules with long alkane-chain could stretch easily, while the polar ester functional group in bio-oil molecules shortens the

intermolecular space. In addition, the cycloalkane rings in the naphthenic-oil rejuvenator enlarge the molecular orientation and tightness, while the condensed aromatic rings in aromatic-oil molecules significantly increase the intermolecular stacking degree [21,25].

However, when the temperature is lower than 213 K, the FFV order changes into NO > AO > EO > BO. At extremely low temperatures, the bio-oil molecules with polar ester groups start to agglomerate together [15,29], and the engine-oil molecules with long alkane chains show a crystallization trend [14], which remarkably reduces the free volume fraction. At the same time, the molecular interaction in naphthenic-oil is much smaller than that in aromatic-oil due to the existence of strong Π-Π stacking between condensed aromatic rings. Fig. 14**b** displays the Connolly surface area of various rejuvenators systems at different temperatures. As the temperature grows, the surface area of rejuvenators increases resulting from the expansion of intermolecular space. At high temperatures, more free volume and surface area would accelerate the penetration and reaction of oxygen and moisture molecules with rejuvenator molecules. Further, the surface area of naphthenic-oil and engine-oil rejuvenators are larger than aromatic-oil, while the bio-oil rejuvenator exhibits the smallest surface area.

7.4. Mean square displacement and diffusion coefficient of different rejuvenators

The molecular mobility and dynamic behaviors of various rejuvenators are predicted and compared. It was reported that molecular mobility was related to low-temperature relaxation and self-healing capacity as well as the diffusion rate of rejuvenators in aged binder [31,42]. The mean square displacement (MSD) of rejuvenator molecules is recorded, which represents the movement distance to the initial position. The MSD results of various rejuvenators at 25℃ are calculated with **Eq.10** and drawn in Fig. 15**a**. It can be found that the MSD value increases gradually with the simulation time prolongs, indicating the self-movement of rejuvenator molecules. Various rejuvenators show the different dynamic behaviors dramatically. The increasing trend of MSD value for bio-oil molecules is the most significant, followed by the engine-oil and naphthenic-oil rejuvenators. Meanwhile, when the simulation time is the same, the MSD value of the aromatic-oil rejuvenator is the smallest. It implies that the bio-oil molecules show the largest mobility, and it is most difficult for aromatic-oil molecules to move around because of the strong intermolecular force between condensed aromatic rings.

$$\mathrm{MSD(t)} = <\Delta \mathrm{r_i(t)}^2> = <[\mathrm{r_i(t)} - \mathrm{r_i(0)}]^2> \tag{10}$$

where MSD(t) is the mean square displacement of rejuvenator molecules at simulation time t (ps), Å^2; $r_i(0)$ and $r_i(t)$ refers to the initial and current coordinate, Å.

From Fig. 15**a**, the MSD parameter of all rejuvenators presents a linear increasing trend as a function of simulation time after 50 ps. To quantitatively compare the dynamic performance of various rejuvenators, the diffusion coefficient indicator is proposed using **Eq.11**.

$$\mathrm{D} = \frac{1}{6\mathrm{N}} \lim_{t\to\infty} \frac{\mathrm{d}}{\mathrm{dt}} \sum \mathrm{MSD(t)} = \frac{\mathrm{a}}{6} \tag{11}$$

where D refers to the diffusion coefficient, m^2/s; N is the total number of rejuvenator molecules; MSD represents the mean square displacement, Å^2; t is the simulation time, s; and a is the slope value in MSD-Time curves.

The calculated diffusion coefficient of four rejuvenators at 298 K is listed in Fig. 15**b**. The magnitude of diffusion coefficient values for different rejuvenators at 298 K varies from 3.21E to 11 to 1.42E-10 (m^2/s), which is higher than the diffusion coefficient of virgin and aged binders (1.92E-11–2.88E-11 m^2/s) [35]. The rejuvenators exhibit a much greater dynamic performance than virgin and aged binders, and that's why these rejuvenators could significantly restore the cracking resistance and viscous performance of aged bitumen [2,6]. Besides, the bio-oil rejuvenator shows the highest diffusion coefficient of 1.417E-10 m^2/s, while the aromatic-oil molecule displays the lowest diffusion coefficient of 3.21E-11 m^2/s. Meanwhile, the diffusion coefficient of engine-oil (1.054E-10 m^2/s) is almost 2 times larger than that of naphthenic-oil (4.87E-11 m^2/s).

7.5. Radius of gyration and radial distribution function of different rejuvenators

The structural characteristics of rejuvenator models are dependent on the rejuvenator molecule type. In this study, the difference in molecular structure and intermolecular order between various rejuvenators is investigated through the radius of gyration (R_g) and radial distribution function (g(r)), respectively. By definition, the R_g represents the initial radius of molecular coils rotating around the center of mass, which reflects the dimensions of the molecule chain. Moreover, the g(r) implies the probability of a specific molecule appearing at a distance from the reference point. The radius of gyration (R_g) and radial distribution function (g(r)) is calculated following **Eq.12 and 13**.

$$\mathrm{R}_g = \left(\frac{\sum r_i^2 m}{\sum m}\right)^{\frac{1}{2}} \tag{12}$$

$$\mathrm{g(r)} = \frac{\mathrm{dN}}{4\pi \mathrm{r}^2 \rho \mathrm{dr}} \tag{13}$$

where the r_i is the distance between the mass center of a molecule to the branch, Å; m is the mass of molecular branch, g/mol; N is molecule number of the whole system; r refers to the distance from the specified

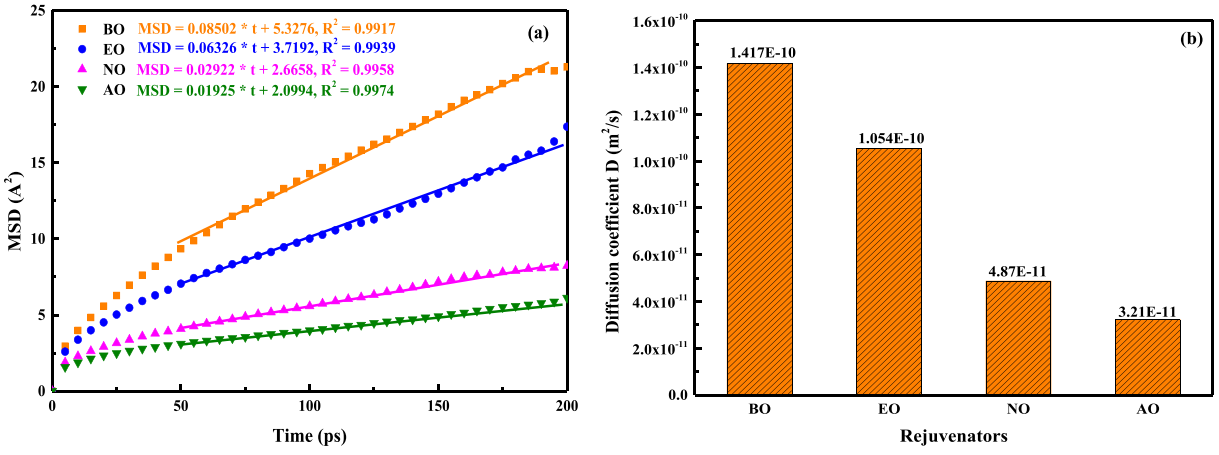

Fig.15. Mean square displacement and diffusion coefficient of various rejuvenators.

molecule, m; and ρ represents the density of rejuvenator model, g/cm^3.

Fig.16a shows the probability density distribution of the R_g for different rejuvenators. Although only one type of rejuvenator molecule is in the simulation model and it seems to be homogeneous, there is a difference in equilibration state between each rejuvenator molecule due to their random arrangement and different atomic interaction environment. Hence, the average molecular model of rejuvenator is not homogenous at the atomic scale. That's why the R_g value of the rejuvenator molecule is not uniform. The probability density distribution of R_g is strongly related to the molecular structure of the rejuvenator. It can be seen that the bio-oil rejuvenator shows the widest R_g region from 3.5 Å to 7.2 Å. The average molecular structure of bio-oil is the straight-chain alkane with 19 carbon atoms, which has a larger R_g value than the mono-cycloalkane (engine-oil), poly-cycloalkane (naphthenic-oil), and polyaromatic (aromatic-oil) molecules. Meanwhile, the long carbon-chain structure in bio-oil leads to numerous configurations and broad R_g distribution. The probability density at R_g of 6.5 Å for bio-oil rejuvenator reaches the maximum point. Besides, the R_g distribution scopes for engine-oil, naphthenic-oil, and aromatic-oil rejuvenators all approach 2 Å, but the R_g value and related probability density are significantly different. In terms of R_g value, the naphthenic-oil is located in 3.5–5.5 Å, while the R_g region for engine-oil and aromatic-oil rejuvenators are the same starting from 4.0 Å to 6.0 Å. Thence, the R_g value of naphthenic-oil molecule is the minimum of 4.5 Å, while the R_g value at peak point for engine-oil and aromatic-oil is about 5.0 Å and 5.3 Å, respectively. The adjacent branched alkane chains in engine-oil and naphthenic limited their R_g values, which is lower than that of aromatic-oil with contrapuntal alkane branches. Meanwhile, the poly-cycloalkane structure in the naphthenic-oil molecule further decreases its R_g value. Based on the peak value of probability density, the aromatic-oil molecule exhibits the highest point at the R_g of 5.3 Å, followed by the engine-oil and naphthenic-oil molecules, while the bio-oil has the lowest peak value. It denotes that the configurations of aromatic-oil and engine-oil rejuvenators are more stable than bio-oil and naphthenic-oil molecules.

The radial distribution function (RDF) of various rejuvenator models is plotted in Fig. 16**b**. The RDF peaks of all rejuvenators mainly occur within the distance of 3.0 Å, after which the RDF value tends to be stable as 1. It means that the rejuvenator molecules are in short-distance order and long-range disorder. The results are consistent with previous MD simulations on bituminous materials [31]. Five common peaks for all rejuvenators at the distance of 1.11 Å, 1.53 Å, 1.77 Å, 2.17 Å, and 2.59 Å can be found, because there is only one type of average molecule in each rejuvenator model and the van der Waals force is the main intermolecular force. The peak values for various rejuvenators are different, and all peak values of the aromatic-oil model are lower than other rejuvenators. On the other hand, one additional peak at 1.35 Å and 1.39 Å for bio-oil and aromatic-oil rejuvenator can be detected. It means that the occurrence probability between bio-oil and aromatic-oil molecules is higher than engine-oil and naphthenic-oil. In other words, there is an agglomeration phenomenon in both bio-oil and aromatic-oil systems. Meanwhile, it should be mentioned that the peak value at 1.35 Å of bio-oil and 1.39 Å of aromatic-oil is 0.45 and 1.39. It demonstrates that the distance between two bio-oil molecules is slightly shorter than aromatic-oil molecules. Moreover, the aggregation degree of aromatic-oil molecules is strongly higher than bio-oil molecules. The existence of polar ester group in the bio-oil molecule and condensed aromatic rings structure in aromatic-oil rejuvenator promote their agglomeration potential. The agglomeration of bio-oil molecules is mainly due to the mutual attraction between polar ester groups in different molecules and the formation of hydrogen bonds. In addition, the aromatic-oil molecules would aggregate together with strong Π-Π stacking interaction [24,34]. Compared to the bio-oil molecule cluster, the distance between aromatic rings is longer than the ester groups, but the intensity of the former is several times stronger than the latter. That's why the additional peak distance and value of bio-oil rejuvenator are both smaller than aromatic-oil molecules. These structural parameters further explain the underlying mechanism in terms of the highest density, potential energy, and cohesive energy density but the lowest fractional free volume and diffusion coefficient of aromatic-oil rejuvenator. Additionally, the last common RDF peak for the aromatic-oil system changes from 2.59 Å to 2.45 Å, which further demonstrates the high agglomeration potential of aromatic-oil molecules.

7.6. Viscosity and activation energy of different rejuvenators

The viscosity is the basic and crucial parameter to assess the fluidity of the rejuvenator, and it was reported that the rejuvenator with low viscosity exhibited the higher rejuvenation capacity on restoring the mechanical properties of aged bitumen [4,9]. Herein, the viscosity values of four rejuvenators at different temperatures are predicted from MD simulations. At the same time, the rotational viscometer is employed to measure the realistic viscosity of rejuvenators. In this study, the viscosity values of four rejuvenators are determined through the Einstein-Stokes equation:

$$D = \frac{kT}{6\pi\eta r} \tag{14}$$

where D is the diffusion coefficient, m^2/s; T (K) and η (Pa·s) show the temperature and viscosity; k represents the Boltzmann constant, 1.38065E-23 J/K; and r is the radius of gyration for rejuvenator molecule, m.

It should be mentioned that both D and r values come from MD simulations outputs. The predicted and measured viscosity values of four rejuvenators at different temperatures are shown in Fig. 17**a and b**,

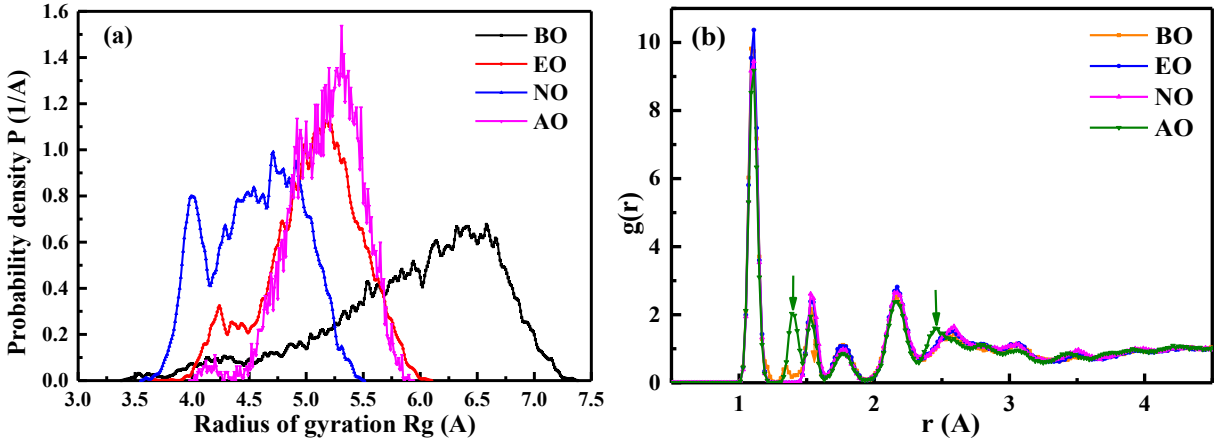

Fig.16. The radius of gyration (a) and radial distribution function (b) of various rejuvenators.

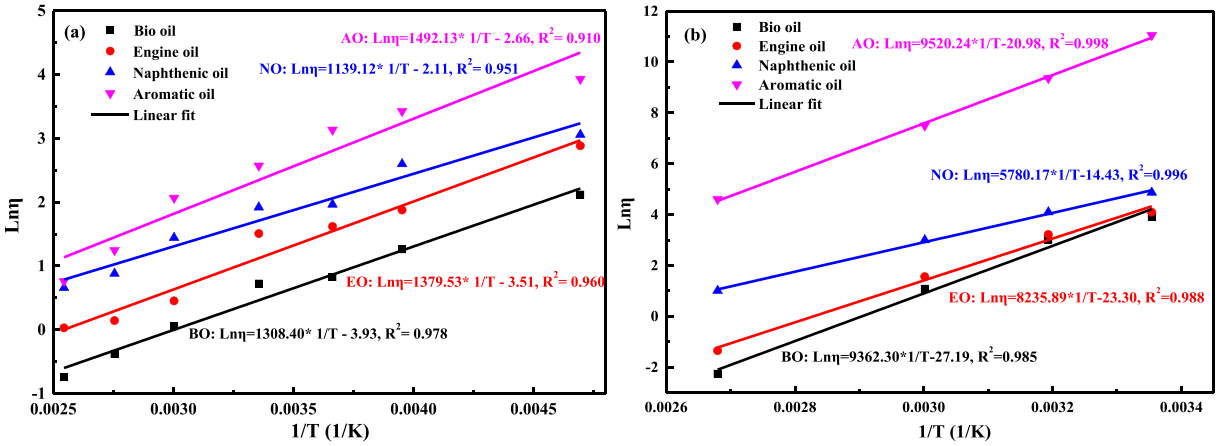

Fig.17. The predicted (a) and measured (b) viscosity of rejuvenators at different temperatures.

respectively. For both MD simulation and experimental results, there is a linearly increasing trend for the (Lnη) parameter of all rejuvenators with the increase of (1/T) value. The bio-oil rejuvenator shows the lowest viscosity, and the engine-oil rejuvenator has a similar viscosity with bio-oil regardless of the testing temperatures. It implies that the bio-oil and engine oil rejuvenators exhibit the best fluidity and softening capacity. Compared with bio-oil and engine-oil rejuvenators, the naphthenic-oil presents a higher viscosity. It is related to the larger molecular weight and movement resistance. In addition, it should be mentioned that the aromatic-oil rejuvenator behaves the highest viscosity than other rejuvenators, which is associated with the largest molecular weight and strongest molecular interaction due to the distinctive aromaticity and polarity. Importantly, the magnitude order of viscosity for four rejuvenators in both MD simulation and experimental results is the same, which is AO > NO > EO > BO. It further validates the reasonability of MD simulation models and settings. However, the difference between the predicted and measured viscosity values is still observed and predicted viscosity is lower than the real value. The reasons may be explained by the existed scale gap and negligence of heavy-weight molecules in the average molecular model, especially for the aromatic-oil.

The correlation curves between the inverse of testing temperatures (1/T) and dynamic viscosity values (η) of rejuvenators are also drawn in Fig. 17. As expected, the increased temperature weakens the intermolecular friction and reduces the viscosity values of rejuvenators. There is the linear relationship between the (1/T) and (Lnη), and it can be described with the Arrhenius equation as follows:

$$\mathrm{Ln}\eta = \frac{E_{vis}}{R} \bullet \frac{1}{T} + \mathrm{LnA} \tag{15}$$

where η refers to the dynamic viscosity value of tested rejuvenator specimen, Pa·s; T is the temperature, K; E_{vis} is the flow activation energy, J/mol; while A and R is the pre-exponential parameter and gas constant, 8.314 J/(mol·K), respectively.

The flow activation energy and pre-exponential factor values from MD simulations and experiments are listed in Table 6. For both MD simulation and experimental results, the aromatic-oil rejuvenator has the highest flow activation energy, while the naphthenic-oil exhibits the lowest value. Meanwhile, the engine-oil and bio-oil rejuvenators show similar flow activation energy and pre-exponential factor. It manifests that the flowability of aromatic-oil is worse than other rejuvenators. Besides, the sequence of pre-exponential factors for four rejuvenators from simulations and tests are the same as NO > AO > EO > BO. Hence, it is concluded that the MD simulation outputs are reliable but still need to be further optimized to obtain the viscosity results of rejuvenators more approaching to measured values.

Table 6
The E_{vis} and A values of four rejuvenators from MD simulations and tests.

Rejuvenators	BO	EO	NO	AO
E_{MD} (J/mol)	10878.04	11469.41	9470.64	12405.57
A_{MD}	1.17E-4	3.09E-4	7.76E-3	2.19E-3
E_t (J/mol)	77838.2	68473.2	48056.3	79151.3
A_t	1.55E-12	7.60E-11	5.41E-7	7.74E-10

8. Conclusions and recommendations

8.1. Main findings from this study

The molecular structures of rejuvenators are of importance to enhance the accuracy of MD simulations outputs and fundamentally understand the underlying rejuvenation mechanism between aged bitumen and various rejuvenators. This study firstly conducts chemical tests to detect the chemical characteristics of four generic rejuvenators. Afterward, the representative average molecular structures of rejuvenators are established and validated. Further, the MD simulations on rejuvenators' models are performed to predict and compare the thermodynamics and structural properties of different rejuvenators. Herein, the main findings are drawn as follows.

(1) From chemical characteristics of functional groups, elements distribution, and average molecular weight, the average chemical formula of bio-oil, engine-oil, naphthenic-oil, and aromatic-oil is derived as $C_{19}H_{36}O_2$, $C_{22}H_{44}$, $C_{26}H_{48}$, $C_{30}H_{40}$.

(2) MD simulations and experimental results both suggest that the density and glass transition temperature of different rejuvenators vary a great deal with the same ranking order of AO > NO > BO > EO. It proves that the established average molecular structures of four rejuvenators are reasonable. However, there is still a certain gap between predicted and measured T_g values, and the predicted T_g values of all rejuvenators are higher than DSC results.

(3) Energetic parameters of rejuvenators are strongly related to the rejuvenator types and temperatures. The aromatic-oil exhibits the highest potential, non-bond, van der Waals and electrostatic energies. Besides, the temperature effects on non-bond and valence energy for all rejuvenators are determined by the van der Waals energy and diagonal energy, respectively.

(4) The van der Waals force plays a dominant role in determining the CED and δ values of rejuvenators. The aromatic-oil exhibits the largest CED and δ values, and the engine-oil presents the lowest values. Besides, the sequence of the FFV parameter for four rejuvenators is observed as EO > BO > NO > AO.

(5) The average molecular model of rejuvenator is not homogeneous at the atomic scale. Meanwhile, the existence of polar ester groups in bio-oil and condensed aromatic rings structure in aromatic-oil promote

their higher agglomeration potential, particularly for the aromatic-oil.

(6) The diffusion coefficient of rejuvenators at 298 K varies from 3.21E to 11 to 1.42E-10 m^2/s, and the temperature increase markedly intensifies the diffusion capacity of rejuvenator molecules. The diffusion coefficient ranking for four rejuvenators is BO > EO > NO > AO. The viscosity ranking for four rejuvenators from both MD simulation and experimental tests is opposite to the diffusion coefficient.

8.2. Recommendations for future works

This study focused on investigating the chemical characteristics, establishing the representative average molecular models, and predicting the important thermodynamics properties of four generic rejuvenators for aged bitumen recycling. The outputs can help us fundamentally understand the difference in chemical, thermodynamics, and nanoscale structural properties between various rejuvenators. In addition, the difference between experimental and MD simulations results is still observed when the average molecular models of rejuvenators are adopted. However, the rejuvenators are complicated with numerous molecule types. Thence, the chemical components characterization and multi-components molecular models of these rejuvenators will be further explored.

CRediT authorship contribution statement

Shisong Ren: Methodology, Investigation, Formal analysis, Writing – original draft, Writing – review & editing. **Xueyan Liu:** Supervision, Writing – review & editing. **Peng Lin:** Resources, Methodology, Supervision. **Sandra Erkens:** Methodology, Supervision. **Yangming Gao:** Methodology, Supervision.

Declaration of Competing Interest

The authors declare that they have no known competing financial interests or personal relationships that could have appeared to influence the work reported in this paper.

Acknowledgments

The first author would thank for the funding support from the China Scholarship Council (CSC, No. 201906450025).

Appendix A. Supplementary data

Supplementary data to this article can be found online at https://doi.org/10.1016/j.fuel.2022.124550.

References

[1] Sun D, Sun G, Du Y, Zhu X, Lu T, Pang Q, et al. Evaluation of optimized bio-asphalt containing high content waste cooking oil residues. Fuel 2017;202:529–40.
[2] Wrobel M, Woszuk A, Ratajczak M, Franus W. Properties of reclaimed asphalt pavement mixture with organic rejuvenator. Constr Build Mater 2021;271:121514.
[3] Yang C, Zhang J, Yang F, Cheng M, Wang Y, Amirkahanian S, et al. Multi-scale performance evaluation and correlation analysis of blended asphalt and recycled asphalt mixtures incorporating high RAP content. J Cleaner Prod 2021;317:128278.
[4] Cong P, Guo X, Mei L. Investigation on rejuvenation methods of aged SBS modified asphalt binder. Fuel 2020;279:118556.
[5] Chen A, Hu Z, Li M, Bai T, Xie G, Zhang Y, et al. Investigation on the mechanism and performance of asphalt and its mixture regenerated by waste engine oil. Constr Build Mater 2021;313:125411.
[6] Hu D, Gu X, Dong Q, Lyu L, Cui B, Pei J. Investigating the bio-rejuvenator effects on aged asphalt through exploring molecular evolution and chemical transformation of asphalt components during oxidative aging and regeneration. J Cleaner Prod 2021;329:129711.
[7] Fallah F, Khabaz F, Kim YR, Kommidi SR, Haghshenas HF. Molecular dynamics modeling and simulation of bituminous binder chemical aging due to variation of oxidation level and saturate-aromatic-resin-asphaltene fraction. Fuel 2019;237:71–80.
[8] Haghshenas HF, Rea R, Reinke G, Yousefi A, Haghshenas DF, Ayar P. Effect of recycling agents on the resistance of asphalt binders to cracking and moisture damage. J Mater Civ Eng 2021;33(10):04021292.
[9] Ren S, Liu X, Wang H, Fan W, Erkens S. Evaluation of rheological behaviors and anti-aging properties of recycled asphalts using low-viscosity asphalt and polymers. J Cleaner Prod 2020;253:120048.
[10] Ren S, Liu X, Lin P, Jing R, Erkens S. Toward the long-term aging influence and novel reaction kinetics models of bitumen. Int J Pavement Eng 2022. https://doi.org/10.1080/10298436.2021.2024188.
[11] Lin P, Liu X, Apostolidis P, Erkens S, Ren S, Xu S, et al. On the rejuvenator dosage optimization for aged SBS modified bitumen. Constr Build Mater 2021;271:121913.
[12] Yan K, Lan H, Duan Z, Liu W, You L, Wu S, et al. Mechanical performance of asphalt rejuvenated with various vegetable oils. Constr Build Mater 2021;293:123485.
[13] M. Gong, J. Yang, J. Zhang, H. Zhu, T. Tong. Physical-chemical properties of aged asphalt rejuvenated by bio-oil derived from biodiesel residue. Construction and Building Materials. 2016, 105, 35-35.
[14] Haghshenas HF, Rea R, Reinke G, Haghshenas DF. Chemical characterization of recycling agents. J Mater Civ Eng 2020;32(5):06020005.
[15] Yu X, Zaumanis M, Santos S, Poulikakos LD. Rheological, microscopic, and chemical characterization of the rejuvenating effect on asphalt binders. Fuel 2014;135:162–71.
[16] Zaumanis M, Mallick RB, Poulikakos L, Frank R. Influence of six rejuvenators on the performance properties of reclaimed asphalt pavement (RAP) binder and 100% recycled asphalt mixture. Constr Build Mater 2014;71:538–50.
[17] Nsengiyumva G, Haghshenas HF, Kim YR, Kommidi SR. Mechanical-chemical characterization of the effects of type, dosage, and treatment methods of rejuvenators in aged bituminous materials. Transp Res Rec 2020;2674(3):126–38.
[18] Haghshenas HF, Rea R, Reinke G, Zaumanis M, Fini E. Relationship between colloidal index and chemo-rheological properties of asphalt binders modified by various recycling agents. Constr Build Mater 2022;318:126161.
[19] Lin M, Shuai J, Li P, Kang X, Lei Y. Analysis of rheological properties and micro-mechanism of aged and reclaimed asphalt based on multi-scales. Constr Build Mater 2022;321:126290.
[20] Chen Z, Pei J, Li R, Xiao F. Performance characteristics of asphalt materials based on molecular dynamics simulation-A review. Constr Build Mater 2018;189:695–710.
[21] Guo M, Liang M, Fu Y, Sreeram A, Bhasin A. Average molecular structure models of unaged asphalt binder fractions. Mater Struct 2021;54:173. https://doi.org/10.1617/s11527-021-01754-2.
[22] Cui L, Xu J, Cen L, Ren M, Cao F. Molecular engineering and modification of FCC slurry oil residue for improving ageing resistance of high quality paving asphalt. Constr Build Mater 2021;299:124234.
[23] Xu G, Wang H. Molecular dynamics study of oxidative aging effect on asphalt binder properties. Fuel 2017;188:1–10.
[24] Ding H, Wang H, Qu X, Varveri A, Gao J, You Z. Towards an understanding of diffusion mechanism of bio-rejuvenators in aged asphalt binder through molecular dynamics simulation. J Cleaner Prod 2021;299:126927.
[25] Yao H, Liu J, Xu M, Ji J, Dai Q, You Z. Discussion on molecular dynamics (MD) simulations of the asphalt materials. Adv Colloid Interface Sci 2022;299:102565.
[26] Peng C, Lu L, You Z, Xu F, You L, Miljkovic M, et al. Influence of silane-hydrolysate coupling agents on bitumen-aggregate interfacial adhesion: An exploration from molecular dynamics simulation. Int J Adhes Adhes 2022;112:102993.
[27] Li R, Leng Z, Yang J, Lu G, Huang M, Lan J, et al. Innovative application of waste polyethylene terephthalate (PET) derived additive as an antistripping agent for asphalt mixture: Experimental investigation and molecular dynamics simulation. Fuel 2021;300:121015.
[28] Sonibare K, Rucker G, Zhang L. Molecular dynamics simulation on vegetable oil modified model asphalt. Constr Build Mater 2021;270:121687.
[29] Chen W, Chen S, Zheng C. Analysis of micromechanical properties of algae bio-based bio-asphalt-mineral interface based on molecular simulation technology. Constr Build Mater 2021;306:124888.
[30] Liu J, Liu Q, Wang S, Zhang X, Xiao C, Yu B. Molecular dynamics evaluation of activation mechanism of rejuvenator in reclaimed asphalt pavement (RAP) binder. Constr Build Mater 2021;298:123898.
[31] Cui B, Gu X, Hu D, Dong Q. A multiphysics evaluation of the rejuvenator effects on aged asphalt using molecular dynamics simulations. J Cleaner Prod 2020;259:120629.
[32] Zhang X, Ning Y, Zhou X, Xu X, Chen X. Quantifying the rejuvenation effects of soybean-oil on aged asphalt-binder using molecular dynamics simulations. J Cleaner Prod 2021;317:128375.
[33] Pahlavan F, Hung A, Fini E. Evolution of molecular packing and rheology in asphalt binder during rejuvenation. Fuel 2018;222:457–64.
[34] Sun W, Wang H. Molecular dynamics simulation of diffusion coefficients between different types of rejuvenator and aged asphalt binder. Int J Pavement Eng 2020;21(8):966–76.
[35] Ren S, Liu X, Lin P, Erkens S, Xiao Y. Chemo-physical characterization and molecular dynamics simulation of long-term aging behaviors of bitumen. Constr Build Mater 2021;302:124437.
[36] Zhang L, Shi Q, Zhao C, Zhang N, Chung K, Xu C, et al. Hindered stepwise aggregation model for molecular weight determination of heavy petroleum fractions by vapor pressure osmometry (VPO). Energy Fuels 2013;27(3):1331–6.
[37] Li DD, Greenfield ML. Chemical compositions of improved model asphalt systems for molecular simulations. Fuel 2014;115:347–56.

[38] Hu C, You G, Liu J, Du S, Zhao X, Wu S. Study on the mechanisms of the lubricating oil antioxidants: Experimental and molecular simulation. Journal of Molecular Liquids. J Mol Liq 2021;324:115099.
[39] Li G, Tan Y. The construction and application of asphalt molecular model based on quantum chemistry calculation. Fuel 2022;308:122037.
[40] Li M, Liu L, Xing C, Liu L, Wang H. Influence of rejuvenator preheating temperature and recycled mixture's curing time on performance of hot recycled mixtures. Constr Build Mater 2021;295:123616.
[41] Ding Y, Huang B, Shu X, Zhang Y, Woods ME. Use of molecular dynamics to investigate diffusion between virgin and aged asphalt binders. Fuel 2016;174:267–73.
[42] Xu G, Wang H. Diffusion and interaction mechanism of rejuvenating agent with virgin and recycled asphalt binder: a molecular dynamics study. Mol Simul 2018;44(17):1433–43.
[43] Kang Y, Zhou D, Wu Q, Liang R, Shangguan S, Liao Z, et al. Molecular dynamics study on the glass forming process of asphalt. Constr Build Mater 2019;214:430–40.
[46] Shan Ke, Bao C, Li D, Zheng C, Aparicio S. Microscopic analysis of the rejuvenation mechanism and rejuvenation effect of asphalt binders. Adv Mater Sci Eng 2021;2021:1–11.